

NRL Report 6314

**Theoretical Interaction Computations for
Transducer Arrays, Including the Effects of
Several Different Types of
Electrical Terminal Connections**

R.V. Baier

*Transducer Branch
Sound Division*

October 7, 1965



**NAVAL RESEARCH LABORATORY
WASHINGTON D.C.**

**APPROVED FOR PUBLIC
RELEASE - DISTRIBUTION
UNLIMITED**

~~CONFIDENTIAL~~
~~UNCLASSIFIED~~

SECURITY

This document contains information affecting the national defense of the United States within the meaning of the Espionage Laws, Title 18, U.S.C., Sections 793 and 794. The transmission or revelation of its contents in any manner to an unauthorized person is prohibited by law.

~~CONFIDENTIAL~~
~~UNCLASSIFIED~~

CONFIDENTIAL
UNCLASSIFIED

CONFIDENTIAL

CONTENTS

Abstract	ii
Problem Status	ii
Authorization	ii
INTRODUCTION	1
DEFINITION OF MUTUAL MECHANICAL IMMOBILITY	1
MATHEMATICAL EQUATIONS	2
EQUATIONS DESCRIBING SPECIFIC TYPES OF ELECTRICAL TERMINAL CONNECTIONS	5
EQUIVALENT CIRCUIT OF A SINGLE ARTEMIS TR-11C TRANSDUCER ELEMENT, INCLUDING PASSIVE ELECTRICAL NETWORK	5
COMPUTED RESULTS	10
Electrical Connections	10
Mass Velocities	10
Spring Displacements	14
Radiated Power	18
Radiation Loads	20
Input Impedances	20
Radiation Load Contours	21
SUMMARY	31
ACKNOWLEDGMENTS	33
BIBLIOGRAPHY	34
APPENDIX A - Relation of a Square Piston to a Circular Piston	37
LIST OF SYMBOLS	38

CONFIDENTIAL
UNCLASSIFIED

ABSTRACT
[Confidential]

Mutual interactions between the elements of a transducer array affect the velocities, radiation loading, directivity patterns, and the internal electrical and mechanical stresses within the individual elements of a given array and element design. The effects are particularly serious and destructive where the individual elements are "close packed" and small in size compared to a wavelength. These interaction effects have been evaluated theoretically so as to include the electro-mechanical properties of each element, the array geometry, and several types of arrangements of the electrical terminals for a λ by λ (square) array composed of 144 individual radiators whose center frequency is 400 cps.

The results of the computations are presented in terms of the theoretical velocities, radiation loading "contours," power radiated, electrical input impedance, and spring displacements. These results are compared for three different types of electrical terminal connections as a function of the driving frequency.

Some of the more interesting results of the computations are the following. The elements located on the perimeter of the array have a much more uniform behavior with respect to frequency than the interior elements. The all-parallel connection, composed of one group of 144 elements all connected in parallel and denoted by (1,144), has the best performance at the lower frequencies, whereas the series-parallel (6,24) and the series-parallel (36,4) connections have the best performance at the high frequencies. All three types of electrical terminal connections are characterized by power absorption from the acoustic field at some frequency, but this effect occurs at different frequencies for the different types of electrical connections. The phases and the magnitudes of the velocities for these elements have rapid changes near the frequency where elements absorb power from the acoustic field. In all cases the series-parallel connection (6,24) is the worst offender.

PROBLEM STATUS

This is an interim report on one phase of the problem; work is continuing.

AUTHORIZATION

NRL Problem S02-07
Project RF 101-03-44-4052

THEORETICAL INTERACTION COMPUTATIONS FOR TRANSDUCER
ARRAYS, INCLUDING THE EFFECTS OF SEVERAL DIFFERENT
TYPES OF ELECTRICAL TERMINAL CONNECTIONS
[Unclassified Title]

INTRODUCTION

The U.S. Navy is engaged in an ASW program which involves a systematic study of sonar detection systems. Much effort for the last few years has been devoted to a 400-cps system known as the Artemis Source. In order to obtain a given power density and to minimize the overall physical size of the transducing element, it was necessary to "close-pack" the individual dipole elements which were employed. A thorough analysis is required to evaluate the effects of acoustic interactions among the elements of a large, low-frequency array composed of small elements close-packed in this manner.

During the past several years many large acoustic arrays have experienced serious and disastrous results, particularly when trying to obtain high power or to control directional power radiation. This difficulty is traced to the acoustic interactions of array elements and to nonlinear element behavior. In an array of radiators, each radiator must work against the acoustic medium reaction force and against the sum of the pressures, or the total interaction force, resulting from all other array radiators. This interaction of one radiator with another is the source of mutual acoustic immobility.

DEFINITION OF MUTUAL MECHANICAL IMMOBILITY

A mathematical expression for the mutual mechanical immobility between two identical circular pistons vibrating in the plane of an infinite rigid baffle has been developed by Pritchard.* His expression forms the basic starting point for the treatment contained in this report. If the radius of the individual pistons is a and the separation between the centers of the pistons is d (Fig. 1), the mutual immobility y_{12} given by Pritchard for $d > 2a$ is

$$y_{12} = g_{12} + j b_{12} = \rho c \pi a^2 \sum_{s=0}^{\infty} \left(\frac{a}{d}\right)^s \sigma_s(ka) \xi_s(kd) \quad (1)$$

where

$$\sigma_s(ka) = 2 \sum_{m+n=s} \frac{\Gamma\left(m+n+\frac{1}{2}\right)}{\sqrt{\pi} m! n!} J_{m+1}(ka) J_{n+1}(ka),$$

$$\xi_s(kd) = \sqrt{\frac{\pi}{2kd}} \left[J_{s+\frac{1}{2}}(kd) + j(-1)^s J_{-s-\frac{1}{2}}(kd) \right],$$

and Γ and J are the gamma and Bessel functions, respectively.

*R. L. Pritchard, "Directivity of Acoustic Linear Point Arrays," Appendix C, Harvard University Acoustics Research Laboratory, Tech. Memo. No. 21, Jan. 15, 1951.

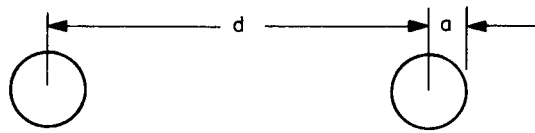


Fig. 1 - Geometry of two identical circular pistons

Figures 2(a) and (b) give plots of the real and imaginary parts, respectively, of the immobility function y_{12} versus the separation between the two pistons and illustrates the oscillatory behavior of this function. The curves of Figs. 2(a) and (b) apply to the cases where $ka = 0.2426, 1.1167, 1.5819,$ and 2.000 and give both the real and imaginary parts of the radiation immobilities for many values of the separation kd of the two pistons. The curves are plotted in dimensionless form so that it is necessary to multiply the ordinate by $\rho c A$ in order to obtain the actual value in the correct units. These curves serve to illustrate the fact that, for elements whose physical size is relatively large (with respect to a wavelength), the interaction impedance coefficients are relatively small compared to the self-load y_{11} of the element. It is obvious that one may obtain the same result with small elements when they are separated by large distances, that is, small interaction load compared to the self-load. For small elements the mutual impedance coefficient is of the order of the self-impedance for close spacing. Therefore, for small, closely spaced elements one may expect to encounter pronounced interaction effects under unfavorable operating conditions.

MATHEMATICAL EQUATIONS

To indicate the general procedure of how one may include the effects of interaction between various radiators, one begins with two identical circular pistons. The net radiation force on the first piston is given by

$$f_1 = y_{11} v_1 + y_{12} v_2, \quad (2)$$

and for the second piston by

$$f_2 = y_{21} v_1 + y_{22} v_2 \quad (3)$$

where y_{11} is the self-radiation immobility which is associated with a single piston in the absence of all other acoustic sources and scatterers, v_1 is the velocity of the first piston, and v_2 is the velocity of the second piston. As the distance of piston 1 to piston 2 is the same as from 2 to 1, $y_{12} = y_{21}$ using Eq. (1), and since the two pistons are identical, $y_{11} = y_{22}$. The net radiation immobility is defined as the net radiation force divided by the velocity of the element; therefore, for piston 1, the net radiation immobility is given by

$$y_1 = \frac{f_1}{v_1} = y_{11} + y_{12} \frac{v_2}{v_1}, \quad (4)$$

and the net radiation immobility for piston 2 is

$$y_2 = \frac{f_2}{v_2} = y_{11} + y_{12} \frac{v_1}{v_2}. \quad (5)$$

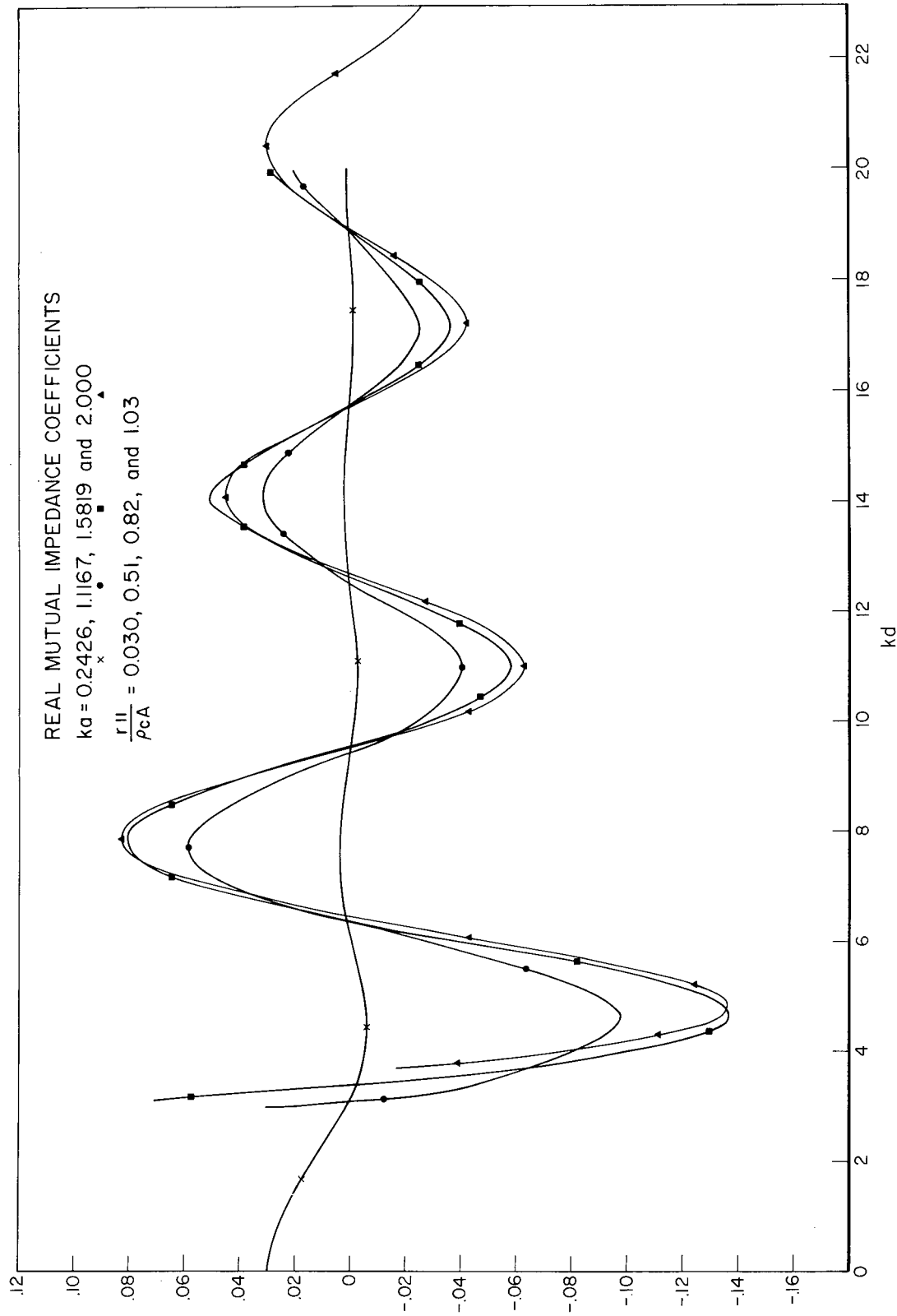


Fig. 2a - Real part r_{12} of the Pritchard mutual mechanical immobility equation r_{12} vs the separation distance kd between two identical circular vibrating pistons

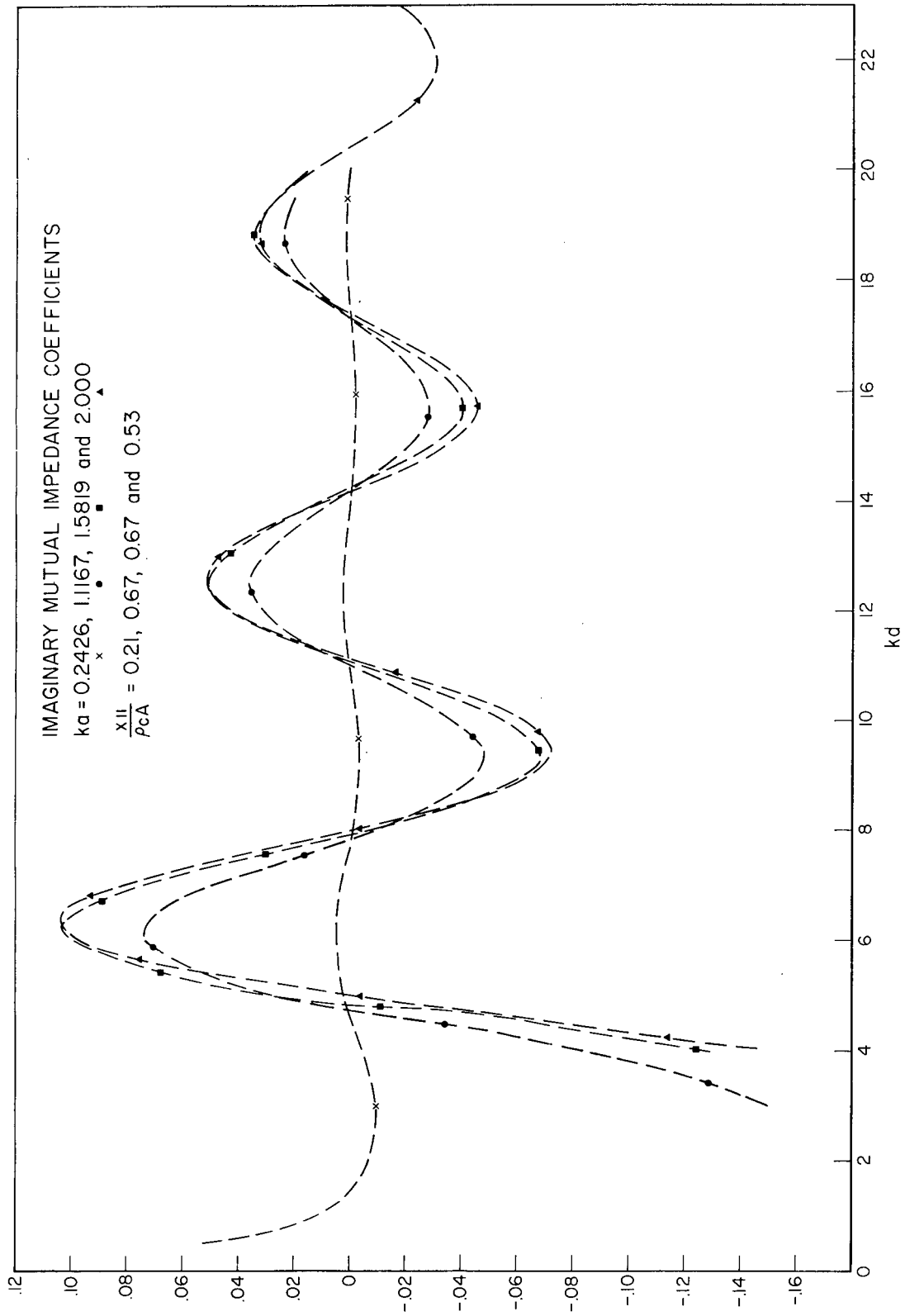


Fig. 2b - Imaginary part b_{12} of the Pritchard mutual mechanical immobility equation \mathcal{V}_{12} vs the separation distance kd between two identical circular vibrating pistons

If there are more than one pair of pistons, then each pair will be considered independently as a first approximation, and the net radiation immobility is given by extending the above equations to include the additional radiators.

It is noted that the symbols y_{11} and y_{12} have been employed for the radiation immobility. This symbolism is based upon the mobility analogy where one chooses the force as analogous to current and the velocity as analogous to voltage. Since this report is concerned only with magnetic-field-type transducers, where the force developed is proportional to the current, it is convenient to use immobility quantities for the mechanical components of the transducer.

EQUATIONS DESCRIBING SPECIFIC TYPES OF ELECTRICAL TERMINAL CONNECTIONS

The following equations are presented in order to illustrate how one may include the interaction effects in an array of radiators, with the inclusion of a passive electrical network in the electrical terminals of each element, and how to drive the radiating elements with three different types of electrical terminal connections. In addition, these equations will include the effects of the mechanical terminals. These elements are considered to be magnetic devices, each of which is representable by an equivalent circuit as shown in Fig. 3.

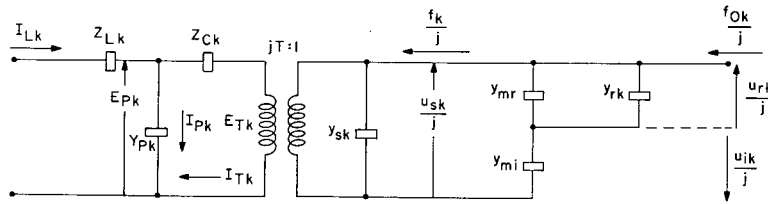


Fig. 3 - Equivalent electromechanical circuit for the radiating device (transducer)

EQUIVALENT CIRCUIT OF A SINGLE ARTEMIS TR-11C TRANSDUCER ELEMENT, INCLUDING PASSIVE ELECTRICAL NETWORK

The equations for a single transducer element are as follows (see Fig. 3):*

$$f_k = -T I_{T k} \tag{6a}$$

$$E_{T k} = T u_{s k} \tag{6b}$$

$$u_{s k} = u_{r k} - u_{i k} \tag{7}$$

$$f_{0 k} = f_k + (y_{m r} + y_{r k}) u_{r k} + y_{s k} (u_{r k} - u_{i k}) \tag{8}$$

$$f_k = y_{m i} u_{i k} + y_{s k} (u_{i k} - u_{r k}) \tag{9}$$

*See List of Symbols at end of report for definition of symbols.

$$I_{Lk} = I_{Pk} + I_{Tk} . \quad (10)$$

Since the only acoustic sources assumed in this problem are those associated with the mutual immobility, the force f_{ok} is neglected. Equations (8) and (9) then yield

$$u_{rk} = \frac{-y_{mi}}{y_{mr} + y_{rk}} u_{ik} , \quad \text{or} \quad u_{ik} = \frac{-(y_{mr} + y_{rk})}{y_{mi}} u_{rk} , \quad (11)$$

and Eqs. (7) and (11) yield

$$u_{sk} = \frac{(y_{mi} + y_{mr} + y_{rk})}{y_{mi}} u_{rk} . \quad (12)$$

Since

$$E_{Pk} = E_{Tk} + I_{Tk} Z_{Ck} , \quad (13)$$

Eqs. (13) and (6b) yield

$$TE_{Pk} = T^2 u_{sk} + TI_{Tk} Z_{Ck} . \quad (14)$$

Combining Eqs. (6a), (7), and (9) give

$$TI_{Tk} = \frac{y_{mi} y_{mr} + y_{sk} (y_{mi} + y_{mr}) + y_{rk} (y_{mi} + y_{sk})}{y_{mi}} u_{rk} . \quad (15)$$

Combining Eqs. (6b), (10), and (13) give

$$\begin{aligned} TI_{Lk} &= T(I_{Pk} + I_{Tk}) = TY_{Pk} E_{Pk} + TI_{Tk} \\ &= TY_{Pk} (E_{Tk} + I_{Tk} Z_{Ck}) + TI_{Tk} \\ &= TI_{Tk} (Y_{Pk} Z_{Ck} + 1) + T^2 Y_{Pk} u_{sk} , \end{aligned}$$

and using Eq. (12) yields

$$\begin{aligned} TI_{Lk} &= \left[Y_{Pk} Z_{Ck} \left(\frac{y_{mi} y_{mr} + (y_{mi} + y_{mr})(y_{sk} + T^2/Z_{Ck}) + (y_{mi} + y_{sk} + T^2/Z_{Ck}) y_{rk}}{y_{mi}} \right) \right. \\ &\quad \left. + \left(\frac{y_{mi} y_{mr} + y_{sk} (y_{mi} + y_{mr}) + (y_{mi} + y_{sk}) y_{rk}}{y_{mi}} \right) \right] u_{rk} . \quad (16) \end{aligned}$$

The preceding derivations are useful for any single element or any number of elements whose electrical terminals are connected in parallel. Now if a series connection of electrical terminals is desired, consider the relationship between the individual element voltages and the voltage across a set of a elements in series. This leads to the following relations:

$$\begin{aligned}
E &= \sum_{k=1}^a E_{Lk} + \sum_{k=1}^a E_{Pk} \\
&= \sum_{k=1}^a I_{Lk} Z_{Lk} + \sum_{k=1}^a I_{Pk} / Y_{Pk} \\
&= \sum_{k=1}^a I_{Lk} Z_{Lk} + \sum_{k=1}^a I_{Tk} Z_{Ck} + \sum_{k=1}^a E_{Tk} \\
&= \sum_{k=1}^a I_{Lk} Z_{Lk} + \sum_{k=1}^a I_{Tk} Z_{Ck} + T \sum_{k=1}^a u_{sk}
\end{aligned} \tag{17}$$

and

$$\begin{aligned}
TE &= T \sum_{k=1}^a I_{Lk} Z_{Lk} + \sum_{k=1}^a \left[\frac{(y_{mi} + y_{mr} + y_{rk})}{y_{mi}} T^2 u_{rk} \right. \\
&\quad \left. + Z_{Ck} u_{rk} \left(\frac{y_{mi} y_{mr} + y_{sk} (y_{mi} + y_{mr}) + y_{rk} (y_{mi} + y_{sk})}{y_{mi}} \right) \right] \\
&= \sum_{k=1}^a T I_{Lk} Z_{Lk} + \sum_{k=1}^a \left[y_{mi} y_{mr} + (y_{mi} + y_{mr}) (y_{sk} + T^2 / Z_{Ck}) \right. \\
&\quad \left. + y_{rk} (y_{mi} + y_{sk} + T^2 / Z_{Ck}) \right] \frac{u_{rk} Z_{Ck}}{y_{mi}}
\end{aligned} \tag{18}$$

As an example, consider a group with six elements in series electrically, and then consider 24 of these groups in parallel. The upper limit a in the above equations would then be equal to six, and E would be the voltage impressed across each of these groups of six elements. This arrangement would develop 1×24 voltage equations, and in each group of six elements the common currents I_{Lk} may be equated to each other, i.e.,

$$I_{L1} = I_{L2} = I_{L3} = I_{L4} = I_{L5} = I_{L6} .$$

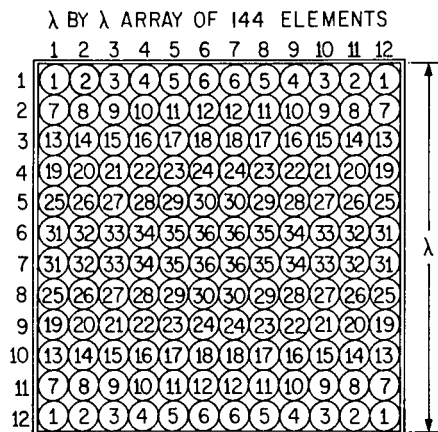
This generates five independent current equations per group of six, or a total of $5 \times 24 = 120$ current equations. Therefore the total number of equations (current plus voltage) is $24 + 120 = 144$ simultaneous complex equations in 144 unknowns. Unfortunately, this model is not completely general and will give a unique description for the following cases investigated: all elements in parallel, i.e., all 144 elements arranged as one group connected electrically in parallel, denoted by the symbol (1,144), all elements in series (144,1), and the series-parallel cases (6,24) and (36,4). One could have made the passive network a T network and this would only add mathematically an impedance to Z_{Ck} such that $Z_{Ck} \rightarrow Z_{0k} + Z_{Ck}$.

CONFIDENTIAL

The following basic assumptions have been applied to the analysis to follow:

1. The expressions derived by Pritchard for the interaction between two circular pistons in an infinite rigid baffle is an adequate first approximation to the interaction between two square pistons having the same volume velocity and no baffle at all (see Appendix A).
2. The shape of the velocity distribution over the surface of any given radiator is not altered by the pressure produced by other radiators which are interacting (that is, linear superposition holds).
3. Those effects which are similar to diffraction phenomena can be neglected for first-order solutions.
4. The transducing elements are linear devices.
5. Reflecting surfaces behind an array of dipoles have a negligible effect on the net radiation load over the surface opposite to a reflector.
6. Holes between the front and back of an array have a negligible effect on the net radiation load.

The transducer element with which this paper is concerned has a magnetic field across an air gap as the source of mechanical force. The electromechanical circuit of one of the elements is presented in Fig. 3. There is a pair of electrical terminals, a term Z_C called "clamped impedance," a quantity associated with the "lumped spring," denoted by y_{sn} , and two velocities u_{rn} and u_{in} . The velocity of the inner mass with respect to an inertial reference is u_{in} and u_{rn} is the velocity of the radiating mass relative to an inertial reference.



PHYSICALLY ASSIGNED SYMMETRY POSITIONS

Fig. 4 - Transducer array containing 144 radiating elements arranged in a square matrix

The transducer array of which these elements are members will be discussed with the aid of Fig. 4. The actual square transducer element has been replaced by the equivalent (equal volume velocity) circular piston, and these elements (144 individual radiators) are "close-packed" into an array whose boundaries are a wavelength on each side.

This paper will present some effects that the electrical terminals have on the behavior of the individual radiators and on the array. In order to observe this effect, three distinct electrical connections for theoretical computations were selected. These three connections are:

1. All electrical terminals are connected in parallel (electrically) to an electrical source of voltage (connection 1).
2. All electrical terminals in one quadrant of the array are connected in series (electrically), and the four quadrants are connected in parallel to an electrical source of voltage (connection 2).

3. The last arrangement consists of 24 groups whose electrical terminals are connected in parallel, with each parallel group containing six elements connected in series (connection 3). These above three electrical terminal connections are illustrated in Fig. 5.

There are 144 radiators in this array, hence 144 simultaneous complex equations in 144 complex unknowns. It was thought desirable to impose certain symmetry conditions on this array due to considerations of cost, computer memory capability, and expediency. In essence, the two-fold symmetry is a division of the array into four identical groups,

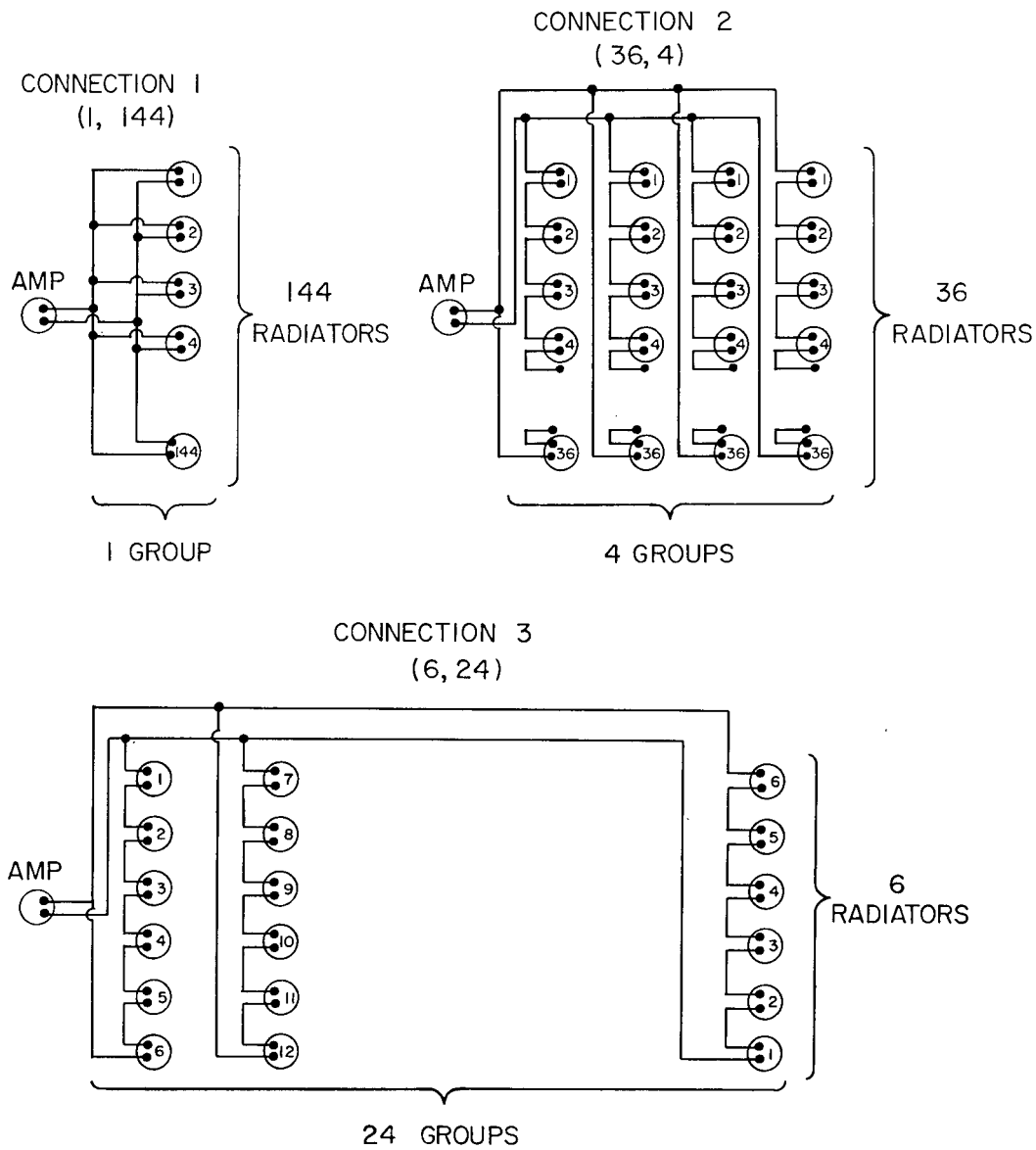


Fig. 5 - Schematic of the three distinct electrical connections considered for the transducer array shown in Fig. 4

as indicated by the repetition of the radiator's number in the circles in Fig. 4. This reduces the number of unknowns by a factor of four so that the solution now involves solving a set of 36 simultaneous complex equations, or 72 simultaneous real equations, in the computer. These computations include the parameters of the circuit describing the mechanical and electrical properties of the individual radiators which were obtained experimentally and located in the array in such a manner as to be in agreement with the symmetry assumed.

COMPUTED RESULTS

Electrical Connections

Connection 1 (parallel connection 1,144) has a fixed voltage (magnitude and phase) impressed across each pair of electrical terminals; the voltage is taken to be 40 volts. Connection 2 (series-parallel connection 36,4) has a fixed voltage impressed across the four parallel groups, each composed of 36 pairs of electrical element terminals connected in series; the voltage is equal to 1440 volts. Connection 3 (series-parallel connection 6,24) has a common voltage impressed across the 24 parallel groups, each composed of six pairs of electrical terminals connected in series; the voltage in this case is equal to 240 volts. The data, such as individual velocities, individual spring displacements, individual power radiated, and the average power radiated, were then adjusted to correspond to a constant amplifier current versus frequency as determined from the data at a frequency of 400 cps and for a given electrical terminal connection. Due to the effects of interactions, the amplifier current is not in a strict one-to-one correspondence among the various electrical connections. As an aid in distinguishing between the name given to a particular electrical terminal connection and the physical connections, begin with "connection 1" having all the electrical terminals connected in parallel, "connection 2" having nearly all terminals connected in series, and "connection 3" as being something in between connections 1 and 2.

The figures given in this report will, unless specifically stated otherwise, refer to comparisons of the three electrical terminal connections previously mentioned.

Mass Velocities

Figures 6 and 7 present the results of the magnitude (cm/sec) and the phase (degrees) of a particular element velocity as a function of the frequency. Data for both the external and the internal mass velocities are given. These data are presented for each of four different positions in the array.

Figures 6(a)-(d) present comparisons of the outer mass velocity for radiator numbers 1, 6, 9, and 36, respectively (see Fig. 4).

Figure 6(a) shows that the corner element has a large smooth response for the connection 2 case as opposed to the small smooth response of the connection 1 case. The response for connection 3 lies between the other two and is rather erratic. Phase comparisons reveal that the phases all lie close together and there is a slow rate of change of phase with respect to the frequency, with the exception of some positions along the frequency axis for the connection 3 case.

Figure 6(b) shows connection 2 to have the smoothest velocity magnitude curve, with a large amplitude at the center of the band, and connection 1 to have a large undesirable

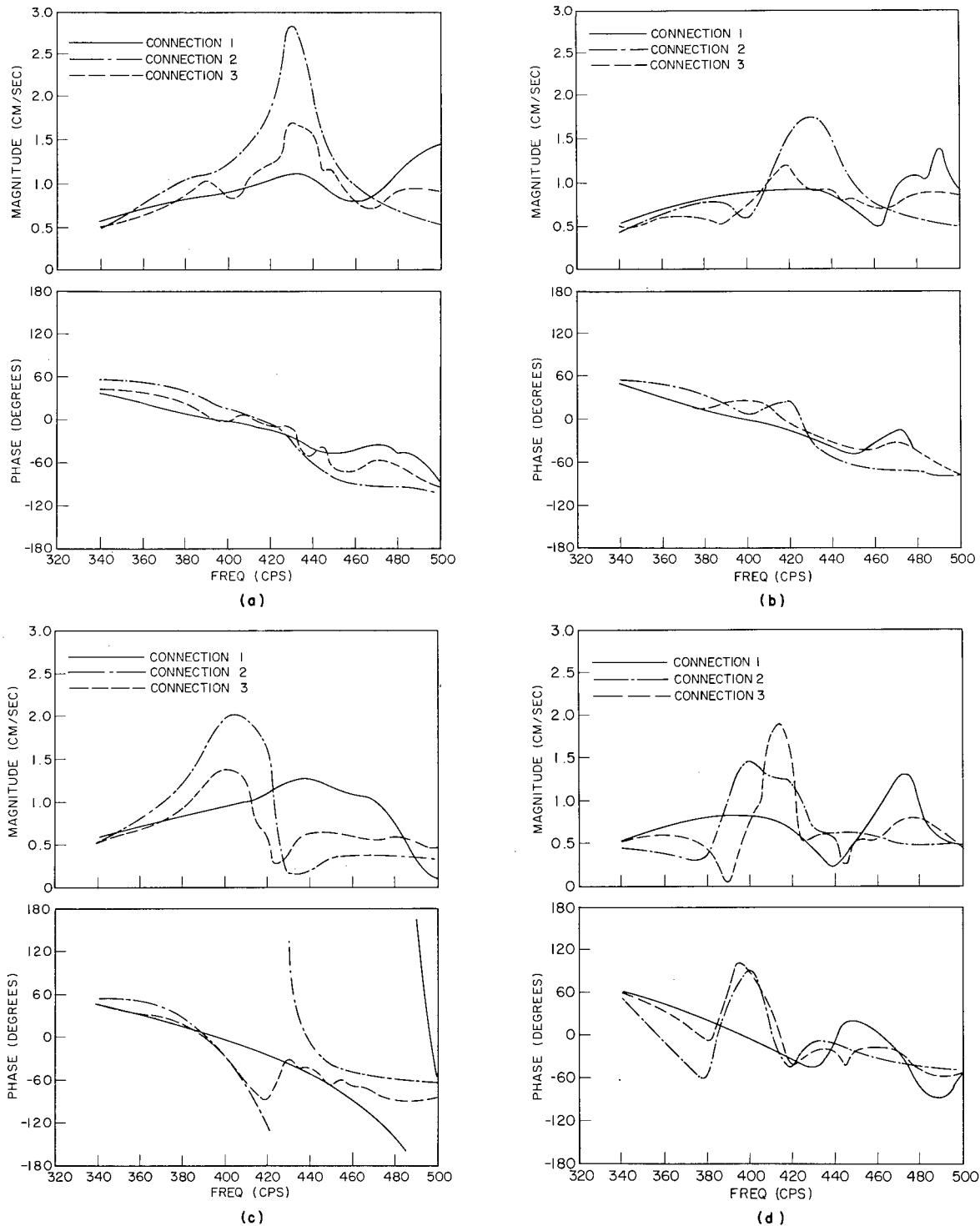


Fig. 6 - Magnitude and phase of the outer mass velocity vs the frequency for four selected radiating transducers. The effect of the type of electrical terminal connection (see Fig. 5) on the velocity data is illustrated for transducer elements (a) No. 1, (b) No. 6, (c) No. 9, and (d) No. 36. The location of these elements in the $144\text{-}\lambda \times \lambda$ array is shown in Fig. 4.

amplitude at the high-frequency end of the scale for radiator No. 6. Comparison of the phases shows that they remain within about 30 degrees of each other over the band of frequencies, with the exception of the bump at 470 cps.

Figure 6(c) shows that the magnitude curves for connection 2 and connection 3 have shifted their peak response to a lower frequency as compared to Fig. 6(a) and (b) and have a sharp cutoff and a moderately flat response above this frequency. The connection 1 curve for radiator No. 9 has shifted its peak response to a higher frequency compared with radiator No. 1 [Fig. 6(a)]. Phase comparisons reveal a rapid change in phase for connection 2 and a small sharp change in phase for connections 1 and 3 at the dip in the respective curves.

Figure 6(d) for radiator No. 36 shows that there is a large dip and a large response at the higher frequencies for connection 1. Connection 3 has two dips and a large response within a rather narrow band of frequencies. Note in the phase curves the similarity between the connection 3 and connection 2 curves. These phase curves have rapid phase changes near the peaks and dips. The connection 1 phase curve is relatively smooth, except at the dip in the corresponding magnitude curve where there is also a rapid change of phase.

Figures 7(a)-(d) present comparisons of the inner mass velocity for radiator numbers 1, 6, 9, and 36.

Fig. 7 - Magnitude and phase of the inner mass velocity for four selected radiating transducers vs the frequency. The effect of the type of electrical terminal connection (see Fig. 5) on the velocity data is illustrated for transducer elements (a) No. 1, (b) No. 6, (c) No. 9, and (d) No. 36. The location of these elements in the $144\text{-element } \lambda \times \lambda$ array is shown in Fig. 4.

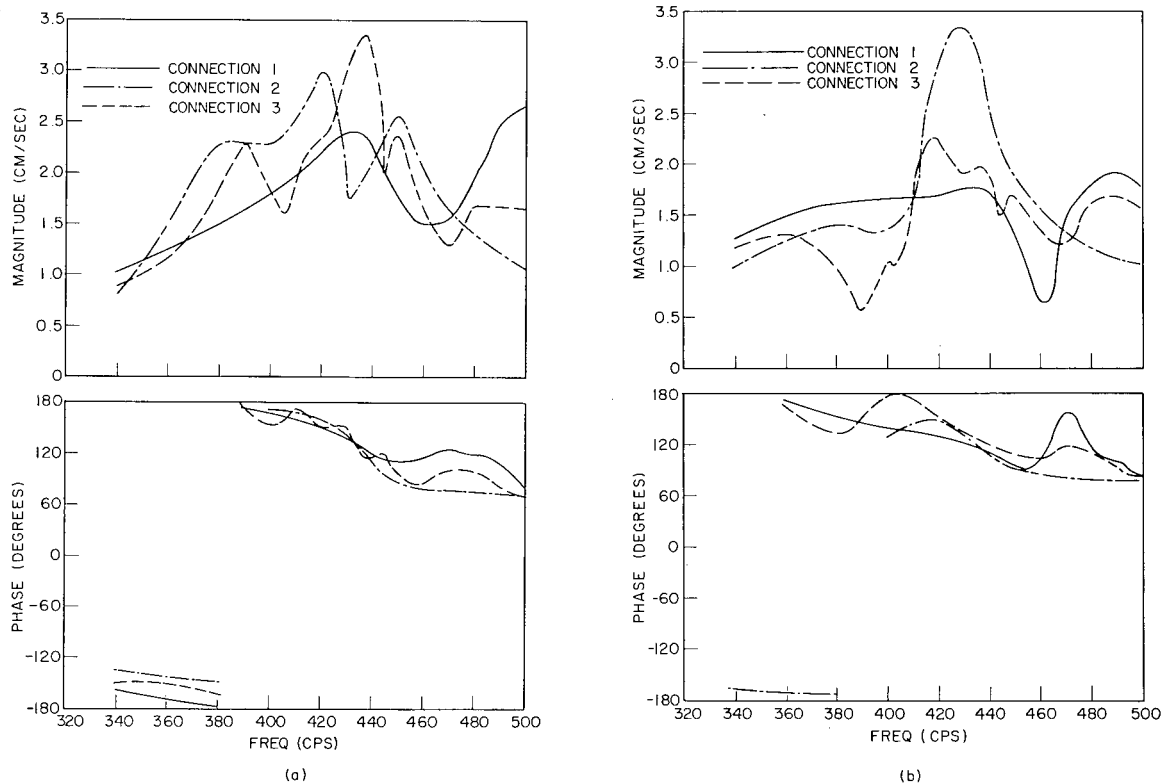
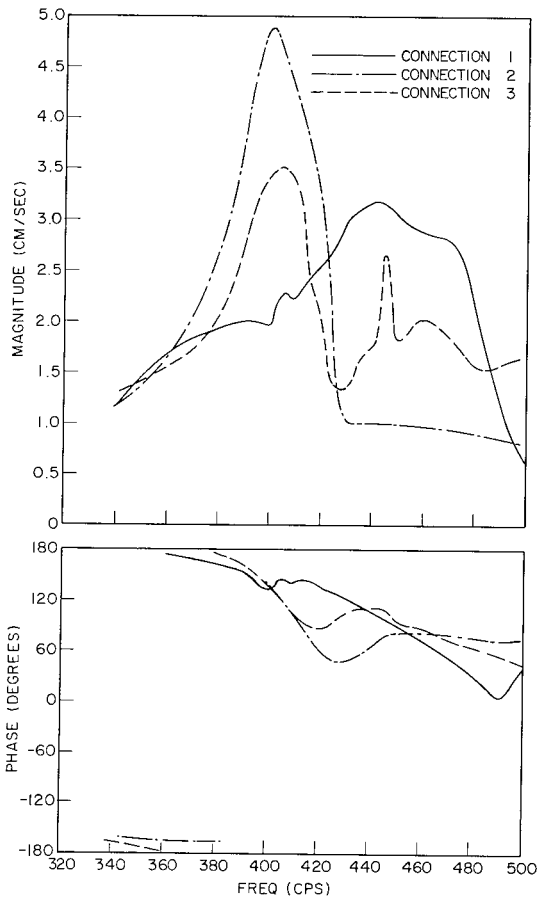


Figure 7(a) presents for radiator No. 1 the magnitude of the internal mass velocity as a function of frequency. The responses for connection 2 and connection 3 are similar in form, shifted with respect to each other on the frequency axis, with connection 1 having the smoothest response. The phases of all three are quite similar, and again connection 3 has some minor phase disturbances.

Figure 7(b) shows that for radiator No. 6 there is a large response which is quite smooth for connection 2. Connection 1 has a uniform response, except for the pronounced dip near the air resonant frequencies. Connection 3 is again quite erratic with a pronounced dip at the lower frequencies. Phase comparisons reveal phase changes for connection 3 at the lower frequencies and phase changes for connection 1 at the higher frequencies.

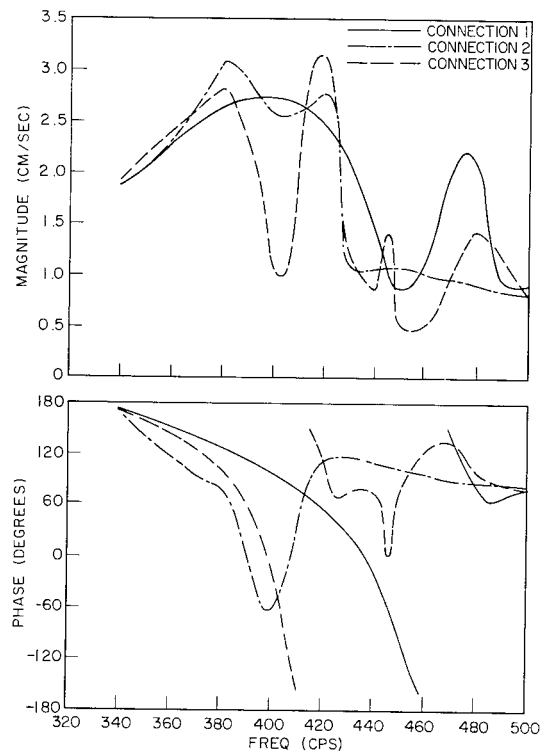
Figure 7(c) presents the response for radiator No. 9. This is the radiator with the largest velocity magnitude in the array. Connection 2 has a sharp cutoff with an ensuing flat response at the higher frequencies, whereas the connection 3 response peaks again. Connection 1 has a relatively smooth response over this frequency band. Connection 2 and connection 3 both have relatively rapid phase changes in the neighborhood of the dip in the response curves.

Figure 7(d) shows that all three of the curves for radiator No. 36 are somewhat misbehaved, with connection 3 being the most serious offender. Note at the frequency at which there is a sharp dip in response that there is a corresponding rapid change in the phase of the velocity. There are dips in the magnitude curve for connection 3 at three distinct



(c)

Fig. 7



(d)

Fig. 7

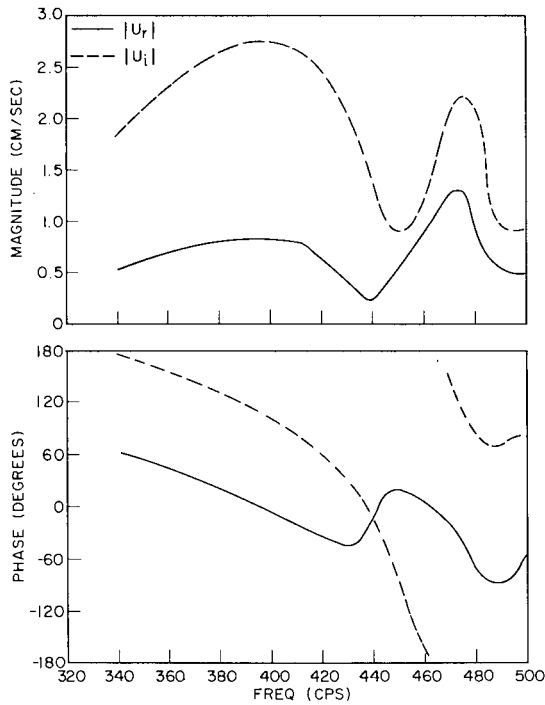


Fig. 8 - Magnitude and phase of the outer (solid line) and inner (dashed line) mass velocities vs the frequency for the transducer located at position No. 36 in the 144-element $\lambda \times \lambda$ array depicted in Fig. 4. These data are for the connection 1 case (all-parallel connection).

the spring displacement are quite similar, with minor changes that correspond to the peaks and dips in the spring displacement magnitudes. The displacement magnitude is somewhat less for radiator No. 6 as compared to radiator No. 1.

Figures 9(c) and (d) present some comparisons of the spring displacements for radiators No. 9 and No. 36. The major displacement peaks have been shifted to a lower frequency as compared to radiators No. 1 and No. 6. In addition, note the steeper slopes in the magnitude, and at the frequencies where the peaks and dips occur, the phases are changing rapidly. The phase change becomes more rapid as the center of the array is approached. The peaks and dips, as well as the rapid changes in phase, are more pronounced for connections 2 and 3.

Tables 1-4 present a comparison of data for the spring displacement (magnitude) as a function of position in the array. Table 1 presents the connection 1, connection 3, and connection 2 cases, from left to right, for a frequency of 390 cps. These data are presented for one-quarter of the array, with the other parts of the array data symmetrically located. Table 2, in the same order, presents data for a frequency of 405 cps. Table 3 presents data for a frequency of 450 cps and Table 4 presents data for a frequency of 480 cps.

frequencies, with corresponding rapid changes in phase. Connection 1 has a large dip and a rapid change of phase at a frequency of 450 cps, which is near the air resonant frequency.

Figure 8 presents a comparison for radiator No. 36 of the magnitude and phases of the external (solid line) and internal (dashed line) mass velocities for the all-parallel connection. Note here the nearly equal amplitudes near the cross-over of the phase at the air resonant frequency.

Spring Displacements

Figures 9(a)-(d) present comparisons of the individual element spring displacement magnitude (mils) and displacement phase (degrees) as a function of frequency for each of four different positions in the array and for the three cases of electrical terminal connections.

Figures 9(a) and (b) present some comparisons of the spring displacements for radiator No. 1 and No. 6, respectively, for the three connections under consideration. The magnitude of the spring displacement is the largest for connection 2. The spring displacements are the most erratic for connection 3. The phases of

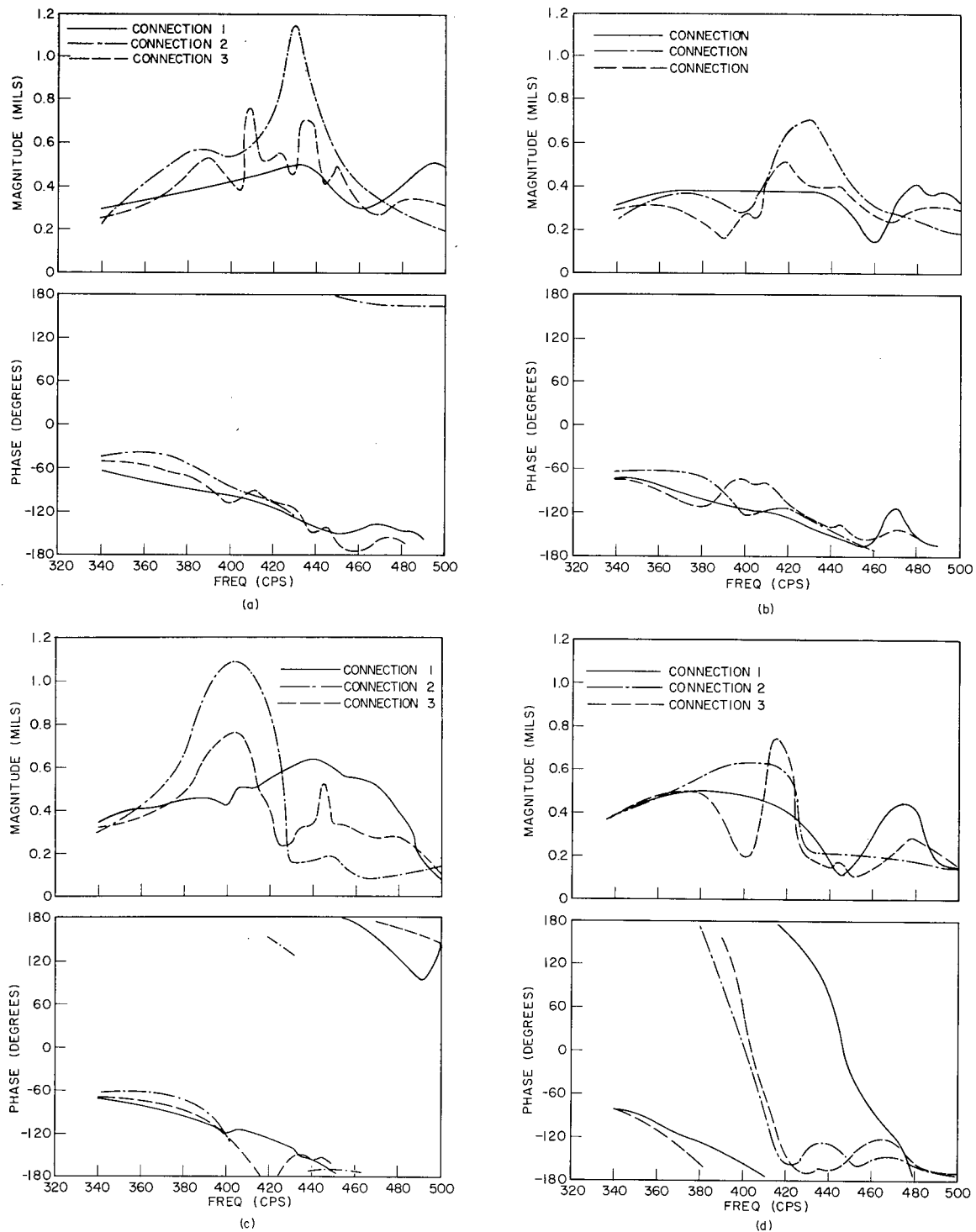


Fig. 9 - Magnitude and phase of the spring displacement for four selected radiating transducers vs the frequency. The effect of the type of electrical terminal connection (see Fig. 5) on the displacement data is illustrated for transducer elements (a) No. 1, (b) No. 6, (c) No. 9, and (d) No. 36. The location of these elements in the $144\text{-element } \lambda \times \lambda$ array is shown in Fig. 4.

Table 1
Distribution of Spring Displacement (Magnitude, Mils)

Frequency 390 cps	Connection 1					Connection 3					Connection 2							
	.40	.42	.41	.40	.39	.38	.53	.59	.51	.39	.24	.16	.64	.76	.72	.64	.51	.44
.43	.44	.46	.44	.42	.43	.43	.66	.65	.64	.39	.25	.11	.84	.87	.95	.71	.53	.47
.39	.42	.44	.47	.45	.46	.46	.57	.63	.59	.48	.23	.17	.63	.72	.72	.67	.40	.31
.42	.43	.46	.46	.46	.47	.47	.75	.71	.63	.39	.22	.64	.72	.68	.61	.38	.19	.17
.38	.41	.43	.46	.47	.48	.48	.70	.71	.57	.40	.28	.30	.53	.51	.36	.18	.22	.35
.37	.44	.45	.47	.50	.50	.50	.63	.84	.64	.40	.31	.37	.43	.51	.31	.15	.38	.55

Table 2
Distribution of Spring Displacement (Magnitude, Mils)

Frequency 405 cps	Connection 1					Connection 3					Connection 2							
	.44	.46	.44	.42	.40	.38	.53	.53	.53	.46	.34	.30	.60	.72	.62	.43	.18	.11
.48	.48	.50	.45	.42	.42	.42	.45	.57	.75	.50	.29	.31	.84	.94	1.14	.74	.38	.19
.42	.44	.45	.47	.43	.43	.43	.34	.53	.67	.68	.30	.30	.50	.74	.92	.99	.47	.25
.44	.44	.45	.44	.42	.43	.43	.51	.66	.79	.53	.19	.24	.51	.68	.85	.64	.30	.15
.39	.41	.40	.43	.43	.44	.44	.47	.69	.70	.54	.17	.22	.22	.39	.43	.33	.22	.38
.36	.43	.43	.44	.46	.46	.46	.40	.88	.85	.54	.12	.32	.09	.31	.33	.22	.45	.70

Table 3
Distribution of Spring Displacement (Magnitude, Mils)

Frequency 450 cps	Connection 1					Connection 3					Connection 2							
	.36	.44	.43	.38	.31	.26	.49	.30	.32	.30	.32	.34	.54	.35	.37	.35	.37	.40
.48	.54	.58	.47	.36	.32	.32	.48	.42	.34	.42	.46	.40	.28	.22	.17	.22	.24	.21
.39	.48	.50	.48	.32	.26	.67	.38	.31	.23	.31	.27	.49	.27	.22	.17	.22	.20	
.42	.46	.45	.33	.19	.11	.35	.29	.24	.28	.31	.29	.27	.21	.18	.21	.23	.22	
.32	.36	.30	.20	.06	.06	.30	.17	.17	.14	.16	.16	.37	.25	.26	.22	.23	.24	
.26	.35	.27	.12	.05	.15	.27	.07	.08	.10	.10	.12	.46	.18	.20	.21	.21	.22	

Frequency 450 cps

Table 4
Distribution of Spring Displacement (Magnitude, Mils)

Frequency 480 cps	Connection 1					Connection 3					Connection 2						
	.40	.38	.26	.25	.33	.40	.34	.29	.30	.30	.31	.32	.27	.22	.22	.22	.23
.50	.44	.38	.20	.26	.42	.35	.32	.28	.30	.32	.30	.21	.18	.16	.17	.18	.17
.27	.27	.22	.15	.09	.26	.24	.17	.14	.12	.13	.13	.25	.19	.17	.15	.17	.16
.36	.24	.12	.10	.07	.16	.11	.08	.06	.06	.06	.06	.20	.17	.16	.16	.18	.17
.32	.25	.08	.06	.16	.26	.18	.14	.14	.14	.15	.15	.23	.19	.18	.17	.18	.18
.32	.42	.23	.15	.30	.42	.38	.27	.27	.28	.28	.29	.25	.17	.17	.17	.17	.18

Frequency 480 cps

Tables 1 and 2 show that connection 1 has a moderately uniform spring displacement magnitude, whereas connection 3 and connection 2 have a variation of about 8:1 throughout the array.

Table 3 shows that connection 1 and connection 3 have variation in the spring displacement of about 10:1, whereas connection 2 has the least variation of about 3:1. The largest spring displacement occurs for the case of connection 3.

Table 4 shows that connection 1 has a variation in the spring displacements of about 8:1, connection 3, a variation of 6:1, and connection 2, a 2:1 variation.

These tables further support the previous data that the all-parallel connections provide the safest spring behavior at the lower frequencies and that connection 2 is the safest at the high frequencies.

Radiated Power

Figures 10(a)-(d) present a comparison of the individual element radiated power as a function of frequency for each of four different radiator positions in the array and for the three cases of electrical terminal connections.

Figure 10(a) for radiator No. 1 reveals the large amount of power radiated over a frequency range of a few cycles for the case of connection 2. The second largest in radiated power over the central part of the frequency band is shown by the curve for connection 3, with the curve for connection 1 having two peaks at the higher frequencies.

Figure 10(b) presents the power curve for radiator No. 6. The radiated power for connection 2 has been reduced, while for connection 1 the output has been increased at the lower frequencies as compared to radiator 1. The power output for connection 3 has been diminished with respect to radiator 1; in addition, there is a severe dip in the curve at 400 cps.

Figure 10(c) presents the power curve for radiator No. 9. This curve shows that for connection 2 the peak output power has shifted to a lower frequency as compared to radiators 1 and 6, and there is a severe dip at 420 cps. At 420 cps this radiator is absorbing power from the acoustic field. The curve for connection 3 has a large peak and dip at 400 and 420 cps, respectively. The curve for the all-parallel connection is rather broad at the lower frequencies and then drops rapidly above 470 cps, until at 483 cps this radiator begins to absorb power from the acoustic field.

Figure 10(d) presents the curve for radiator No. 36. Connection 2 and connection 3 curves have large dips at 400 cps (going negative) and large narrow peaks at 420 cps. Connection 1 has a large, smooth radiated power curve below 430 cps, while above 430 cps this radiator absorbs power from the medium over a 25-cycle frequency band centered about the air resonant frequency.

Figure 11 presents a comparison of the average power radiated per element of the array as a function of the frequency for the three cases of electrical connection. Connection 1 has the lowest Q and lowest radiated power while connection 2 has the highest Q and highest radiated power per unit current input.

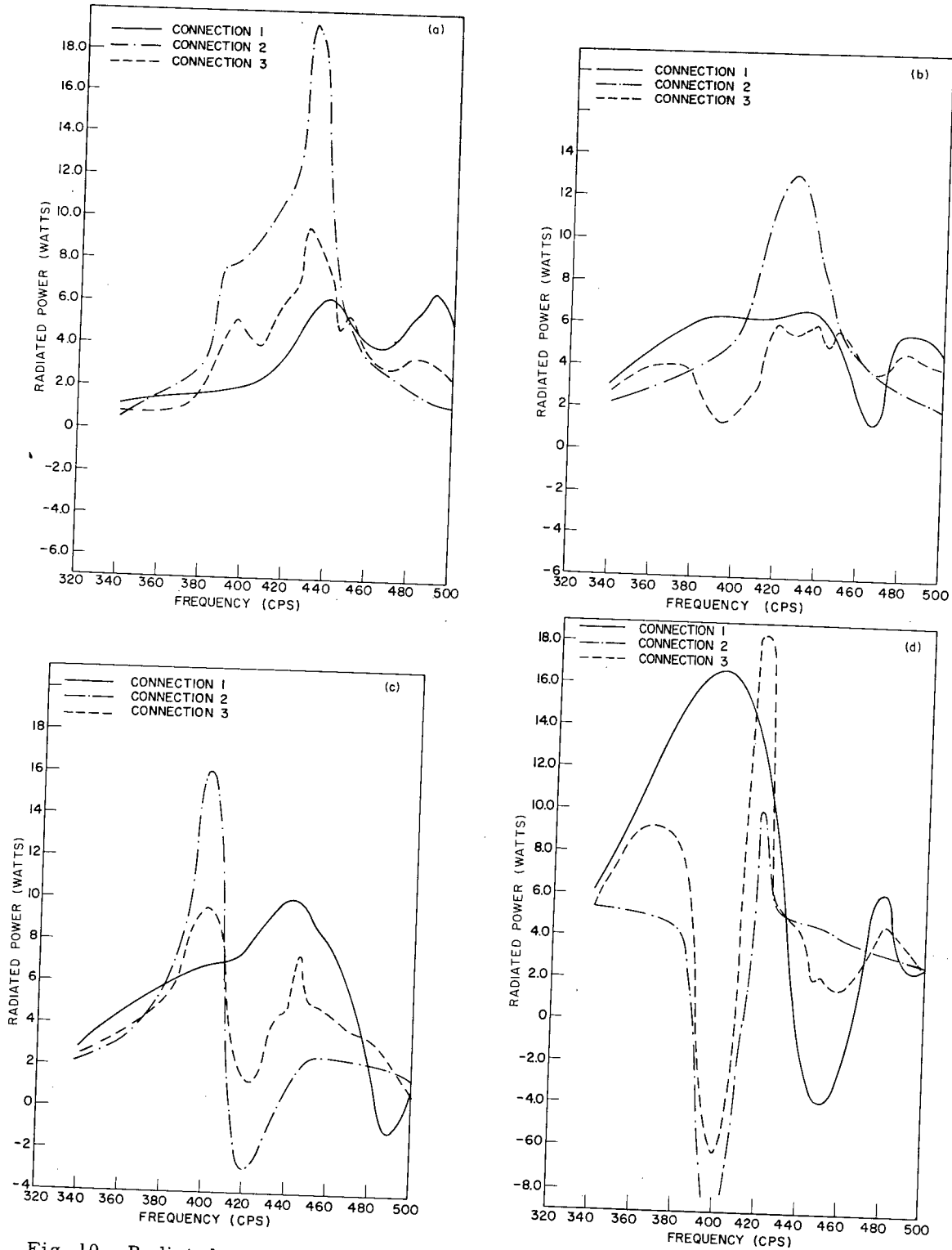


Fig. 10 - Radiated power vs frequency for four selected radiating transducers. The effect of the type of electrical terminal connection (see Fig. 5) on the radiated power is illustrated for transducer elements (a) No. 1, (b) No. 6, (c) No. 9, and (d) No. 36. The location of these elements in the $\lambda \times \lambda$ array is shown in Fig. 4.

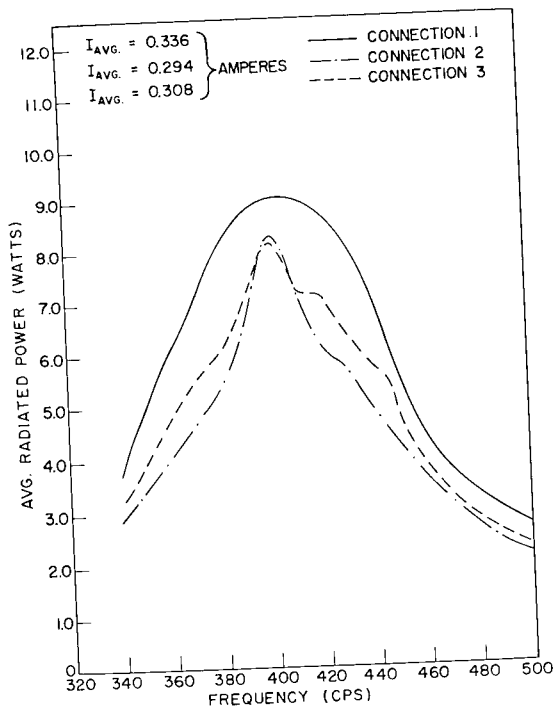


Fig. 11 - Average power radiated by each element of the 144-element array as a function of the frequency. The effect of the type of electrical terminal connection on the power radiated is illustrated.

Radiation Loads

Figures 12(a) and (b) present a comparison of the average real and imaginary components, respectively, of the radiation load as a function of the frequency. Note in Fig. 12(a) that the "hole" in all three cases covers approximately the same width in cps. One notes that connection 1 (all parallel) presents a uniform load for the real component for frequencies less than 440 cps and that connection 3 presents a rather erratic radiation load at nearly all frequencies.

Figure 12(b) presents an extremely erratic behavior of the imaginary component of radiation load for connection 3 case, particularly between 380 and 430 cps. The all-parallel connection (i.e., connection 1) has a uniform load from 340 to 430 cps, and above 430 cps it has a rather disturbing variation. Connection 2 has a more moderate variation in the reactive load as a function of frequency.

Input Impedances

Figures 13(a)-(d) present the components of the input impedance at the electrical terminals of each element. The units on the axes are the practical ohm for both the resistance R and the reactance X parts of the impedance.

Figure 13(a) presents the impedance with the frequency (cps) as a parameter for radiator No. 1. Note for connection 1 the moderately well behaved impedance curve containing a small loop near the upper end of the frequency scale. Connection 2 and connection 3 both have many of these small loops at several frequencies, with the consequence of the impedance curve being a distorted circle. All of the curves reveal a lightly loaded condition for this corner element.

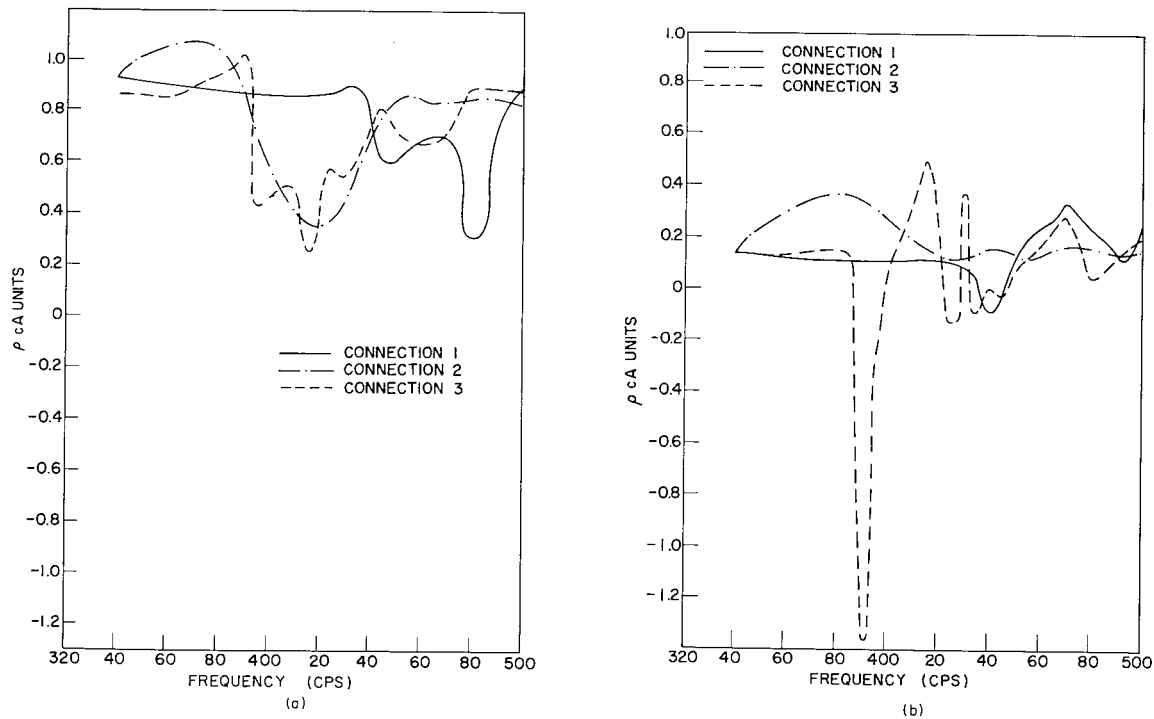


Fig. 12 - Average radiation load vs the frequency for each element of the 144-element array. The data shown are for (a) the real part and (b) the imaginary part of the radiation load. The ordinate axes are given in units of ρcA . The effect of the type of electrical terminal connection on the radiation load is illustrated.

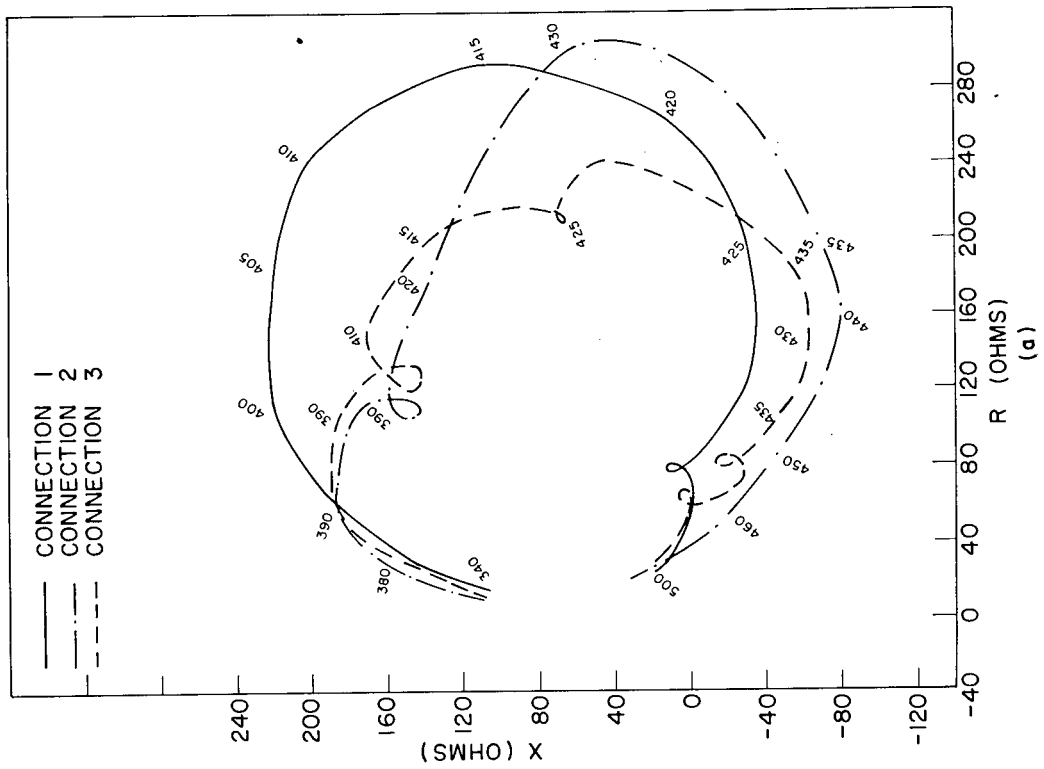
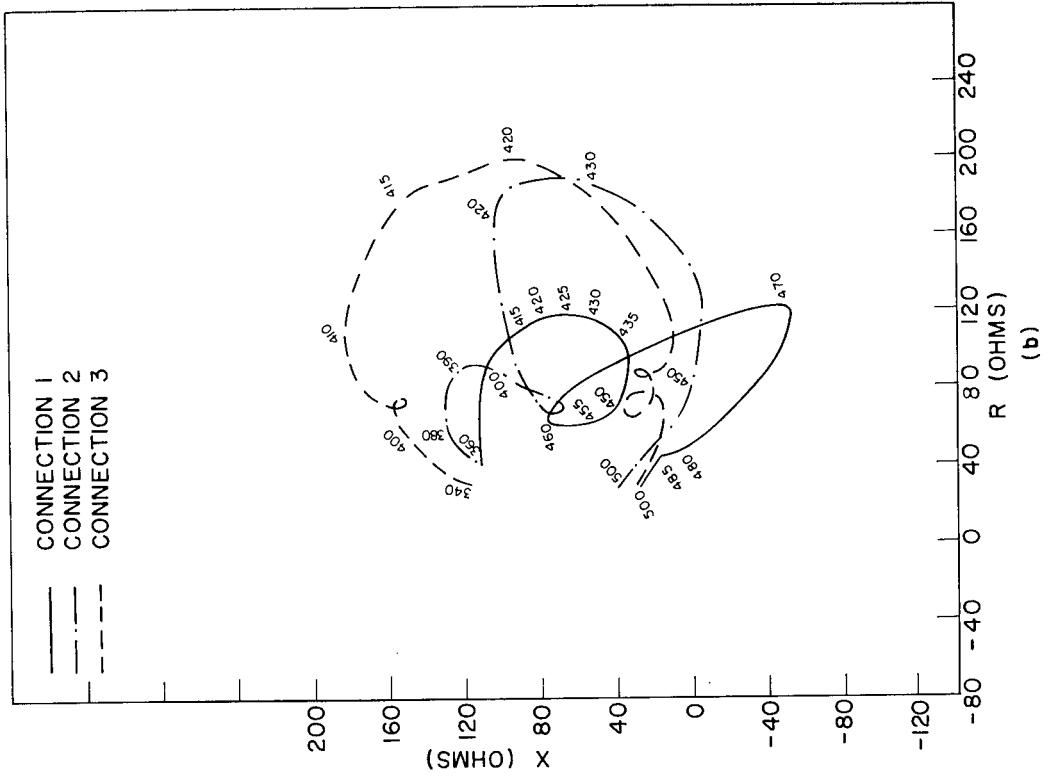
Figure 13(b) gives the impedance curve for radiator No. 6. Note the reduction in size of the curve when compared to Fig. 13(a). Connection 1 has a very distorted curve. Connection 3 curve reveals the lightly loaded condition, resulting in a more nearly circular plot.

Figure 13(c) presents the impedance curve of radiator No. 9. Connection 1 and connection 3 curves are more nearly circular, with connection 2 indicating a lighter load and, at some frequencies, having negative resistance values as well as negative reactance values.

Figure 13(d) presents the curves of the impedance for radiator No. 36. The curve for connection 1 has its major part in the negative resistance and reactance quadrants of the impedance plot. In fact, all three curves have negative resistance values, with connection 3 curve indicating the heaviest positive load at the mechanical terminals.

Radiation Load Contours

Connection 1 - Figures 14-16 present the real and imaginary parts of the radiation load "contours," in dimensionless units, for the all-parallel connection. The diameter of the individual transducer elements is $2a$, and the sides of the array are $2x$. The value assigned to each radiation contour is given to only one decimal place and was obtained by dropping all digits beyond the first decimal place. For example, all radiation load values



between 0.3 and 0.4 were assigned the value 0.3; all values between 0.0 and -0.1 were assigned the value -0.0, etc.

The points on the figures define the centers of the individual elements, and contour lines enclose points of equal assigned values.

Figure 14(a) presents the real part of the radiation load when the array is driven at a frequency of 340 cps. There is a progressive increase in the radiation load from a low value at the corner to a high value at the center of the array. The radiation load pattern has a sort of circular symmetry. The corresponding velocity distribution (external velocity) is highest for the outer elements and smallest in the interior, with a total maximum variation of approximately 10 percent where the average is 0.55.

Figure 14(b) presents the imaginary part of the radiation load. The central part of the array has essentially a zero reactive load and increases away from the center toward an edge. The phase angle of the velocity is highest at the center of the array and falls off toward an edge. There is a total variation in velocity phase angle of about 25 degrees where the average phase angle is about 50 degrees.

Figure 15(a) presents the real part of the radiation load when the array is driven at a frequency of 400 cps. There is a progressive increase in the radiation load from an edge toward the center, with a larger variation in the extreme values as compared to the 340-cps pattern. Note that the pattern is broken up into rather small pieces. The velocity distribution is not as uniform as the 340-cps pattern, with the high values still on the outside edge and a total variation of approximately 15 percent where the average is 0.86.

Figure 15(b) presents the imaginary part of the radiation load. In the corners the imaginary part of the radiation load is positive and nearly uniform, falling off toward the

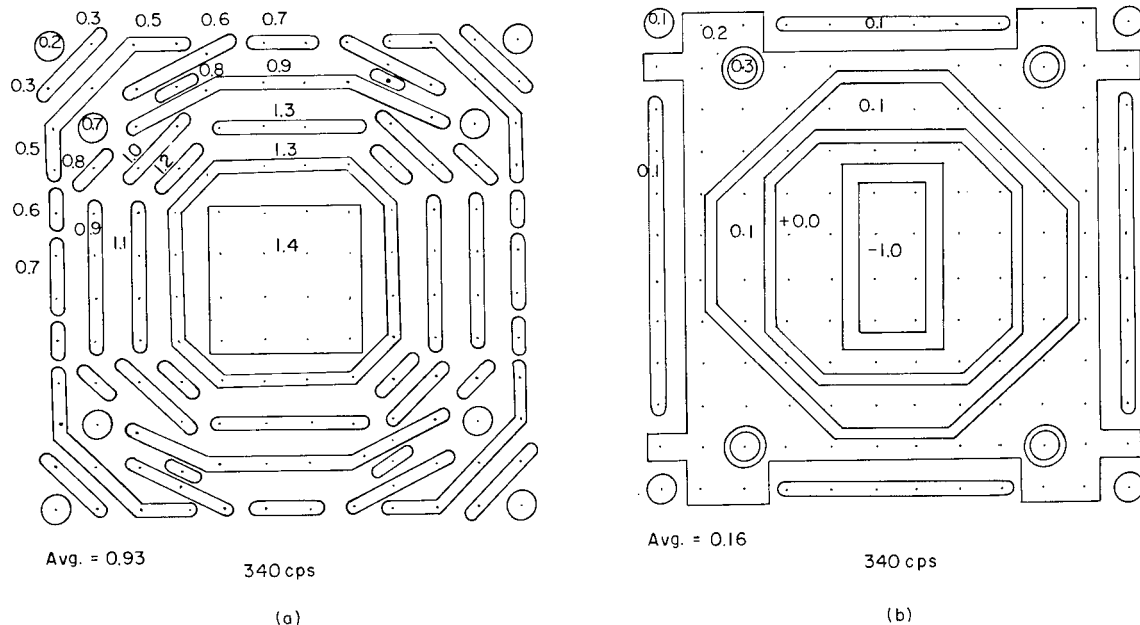


Fig. 14 - Contours of the (a) real and (b) imaginary parts of the radiation load for the 144-element array driven at 340 cps. The dots represent the positions of the transducer elements in the array. The data are for the connection 1 case (see Fig. 5).

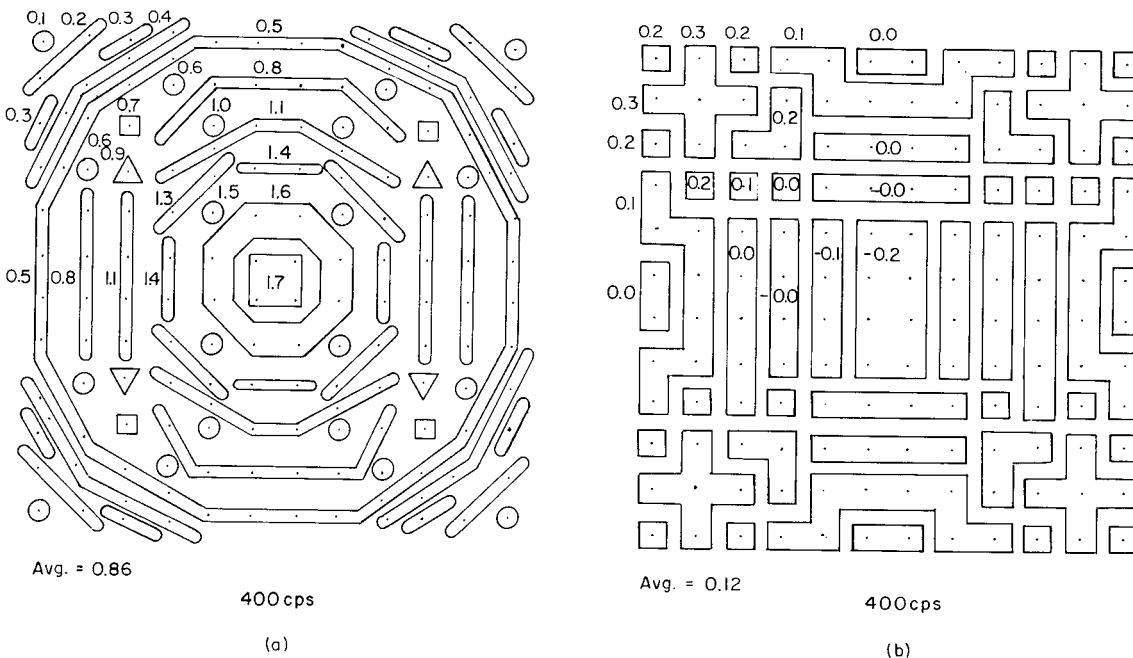


Fig. 15 - Contours of the (a) real and (b) imaginary parts of the radiation load for the 144-element array driven at 400 cps. The dots represent the positions of the transducer elements in the array. The data are for the connection 1 case (see Fig. 5).

interior and becoming negative near the center of the array. The phase angle of the velocity is nearly uniform throughout the array, with an average of 356 degrees.

Figure 16(a) presents the real part of the radiation load when the array is driven at a frequency of 450 cps (the air resonant frequency). There is a progressive increase in the value of radiation load from an edge toward the center, and then near the center the load becomes negative. The velocity distribution is still highest for the outer elements, with a total variation in magnitude of 60 percent and an average of 0.77.

Figure 16(b) presents the imaginary part of the radiation load. Here, one observes a rather chaotic pattern, with large variations in loading existing throughout the array and with a considerable portion of the center elements having large negative values. The phase angles of the velocities among the elements of the array have a maximum variation of about 90 degrees and an average of 320 degrees.

Connection 3 - Figures 17-19 present the real and imaginary part of the radiation load "contours" for the connection 3 case.

Figure 17(a) presents the real part of the radiation load when the array is driven at a frequency of 340 cps. There is a progressive increase in the radiation load from an edge toward the center, similar to the all-parallel case. There is not the same high degree of symmetry as is evident in the all-parallel case. There is approximately a 3:1 variation across the array in the values of the radiation load. The variation along the diagonal is approximately equal to the square of the variation along an edge. There is a variation of approximately 10 percent in the magnitude of the velocities where the average velocity magnitude is 0.50.

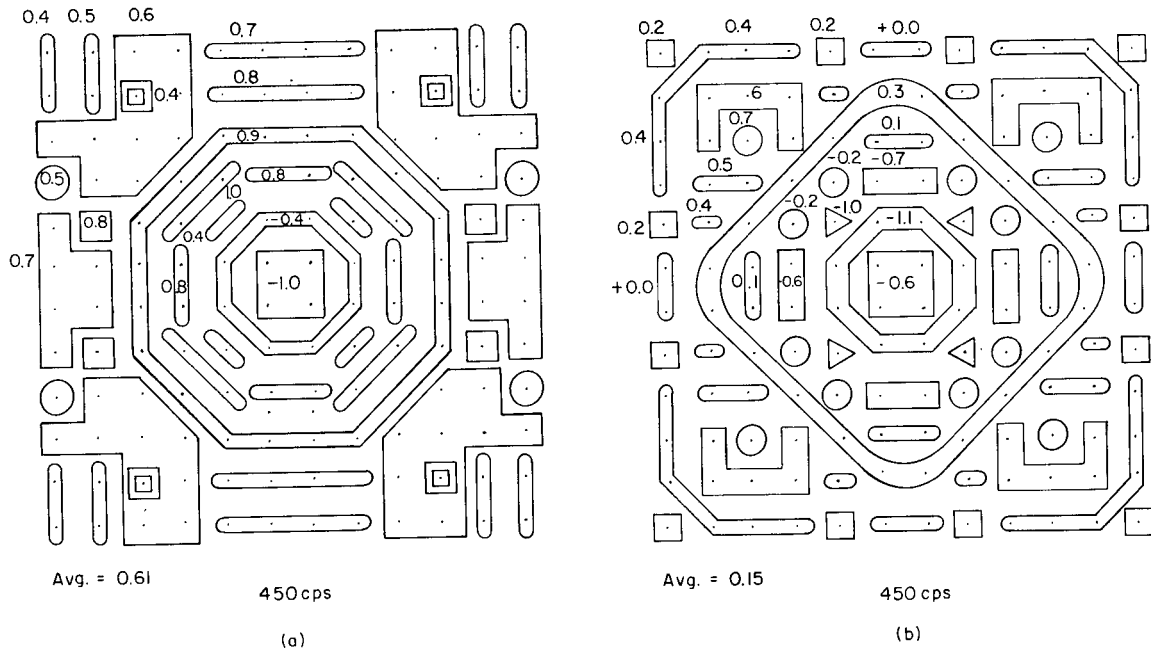


Fig. 16 - Contours of the (a) real and (b) imaginary parts of the radiation load for the 144-element array driven at 450 cps. The dots represent the positions of the transducer elements in the array. The data are for the connection 1 case (see Fig. 5).

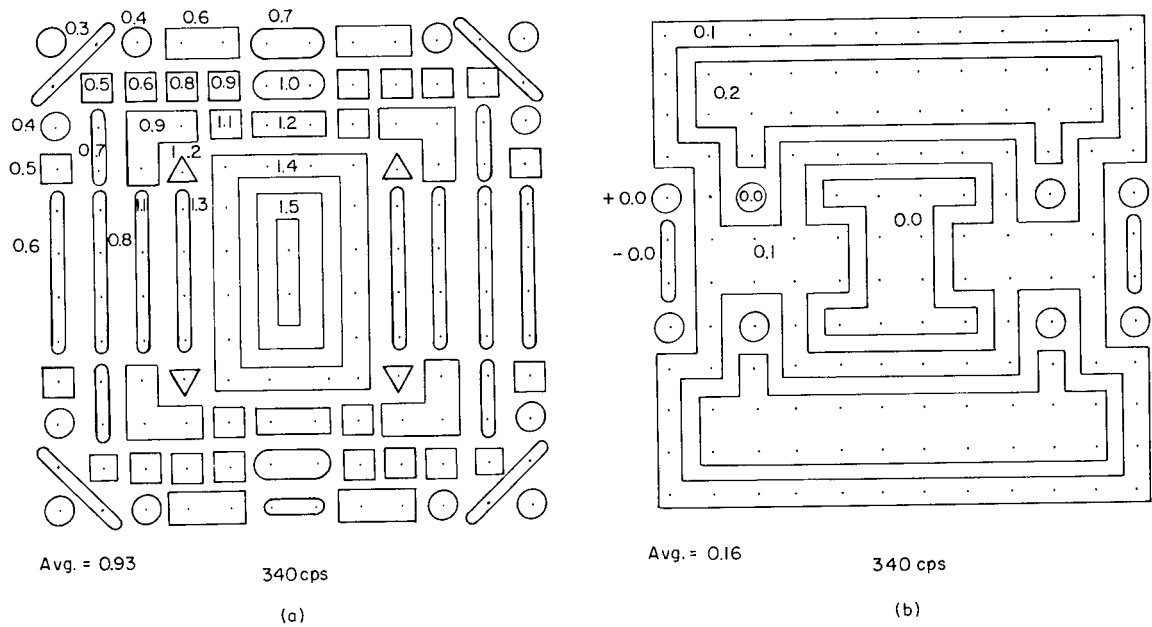


Fig. 17 - Contours of the (a) real and (b) imaginary parts of the radiation load for the 144-element array driven at 340 cps. The dots represent the positions of the transducer elements in the array. The data are for the connection 3 case (see Fig. 5).

CONFIDENTIAL

Figure 17(b) presents the imaginary part of the radiation load. The values for the edge elements are small, increasing toward the center and then reversing, falling to zero at the center. The phase angle of the velocity is highest at the center of the array with a maximum variation of 16 degrees. The average phase is 52 degrees.

Figure 18(a) presents the real part of the radiation load when the array is driven at a frequency of 400 cps. There appears to be no well-defined pattern for this "contour," with the values being similar to the 450-cps all-parallel connection [Fig. 16(a)]. This contour has a lower degree of symmetry than any of the all-parallel patterns. The average value here is less than the all-parallel average. The velocity distribution is somewhat erratic with respect to position in the array, and in general the larger values are located at the edges with a total variation of about 70 percent. The average velocity magnitude is 0.98.

Figure 18(b) presents the imaginary part of the radiation load. The values at the edges are not as uniform as the all-parallel case, and the central element values have become larger negatively. In addition, this pattern is not as symmetric as the 400-cps all-parallel case [Fig. 15(b)]. The phase angles of the velocities are very erratic, with a total variation of 111 degrees. The average phase angle is 214 degrees.

Figure 19(a) presents the real part of the radiation load when the array is driven at a frequency of 450 cps. Although all values are now positive, there is still considerable distortion in the pattern. The outer elements of the array have the lower values of load increasing toward the center of the array, then near the center the value of the load drops. The average load is larger than the 400-cps all-parallel connection [Fig. 15(a)]. The average value for the magnitude of the velocity is 0.69, with a total variation of about 74 percent.

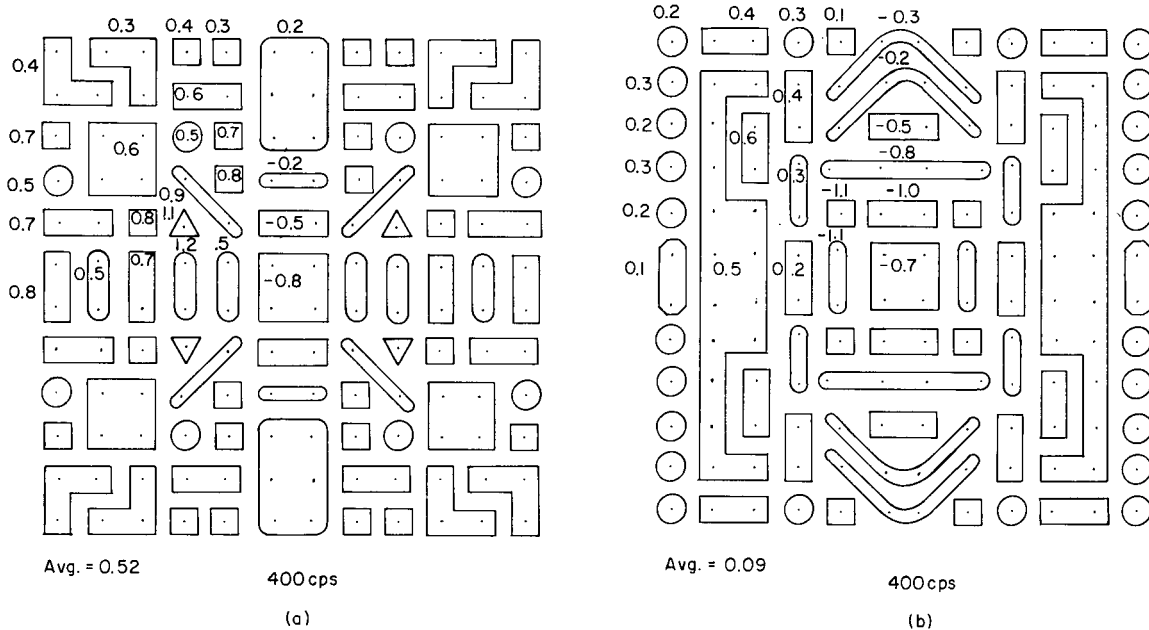


Fig. 18 - Contours of the (a) real and (b) imaginary parts of the radiation load for the 144-element array driven at 400 cps. The dots represent the positions of the transducer elements in the array. The data are for the connection 3 case (see Fig. 5).

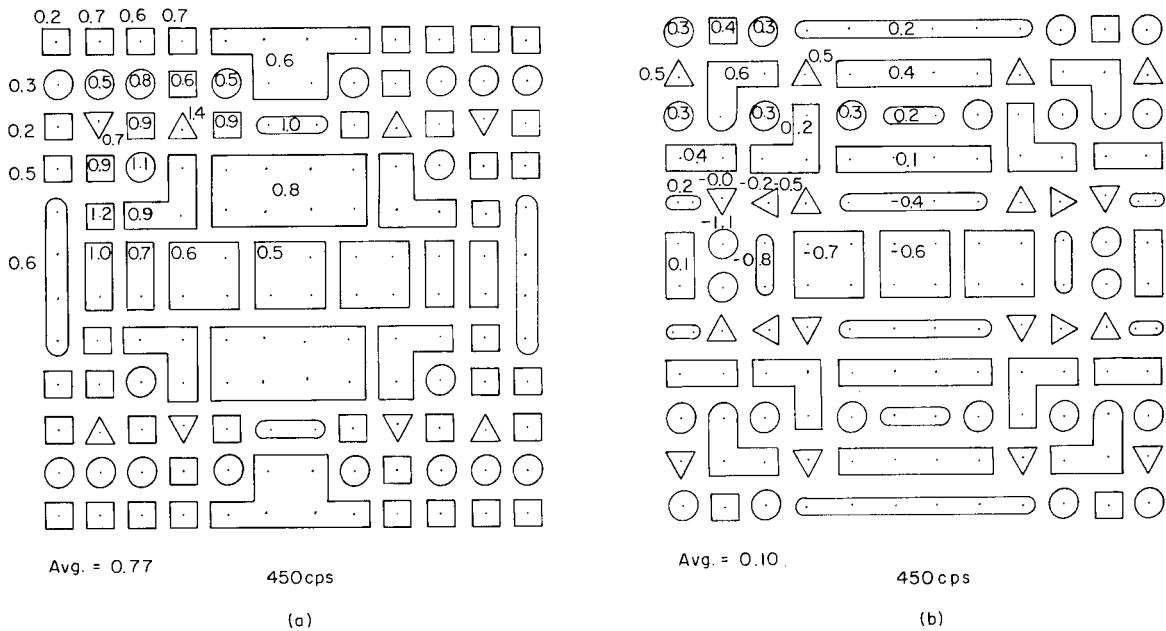


Fig. 19 - Contours of the (a) real and (b) imaginary parts of the radiation load for the 144-element array driven at 450 cps. The dots represent the positions of the transducer elements in the array. The data are for the connection 3 case (see Fig. 5).

Figure 19(b) presents the imaginary part of the radiation load. The outer elements have the higher radiation load, with the central part of the array being negative. The phase angle of the velocities have a variation of 56 degrees. The average phase angle for the velocities is 293 degrees.

Connection 2 — Figures 20-22 present the radiation "contours" for connection 2.

Figure 20(a) presents the real part of the radiation load when the array is driven at a frequency of 340 cps. There is a progressive increase in value from the edge of the array toward the center, with a resulting overall variation of an order of magnitude. The magnitude of the velocities is uniform throughout the array.

Figure 20(b) presents the imaginary part of the radiation load. There is a large uniform section in the central part of the array increasing in value toward the edge, then falling off again at the outer edge. The phase angle of the velocity is quite uniform.

Figure 21(a) presents the real part of the radiation load when the array is driven at a frequency of 400 cps. Note the similarity with the 400-cps connection 3 plot [Fig. 18(a)]. The extremes in the negative values are not as great and the pattern is more symmetric than connection 3. The average value for connection 2 is larger than the average value for connection 3. The distribution of velocities shows that the higher velocity radiators are now located on and near the major diagonal.

Figure 21(b) presents the imaginary part of the radiation load. This plot is similar to the 400-cps connection 3 plot [Fig. 18(b)] of radiation load and again does not have such extremes in the values of the reactive load. The pattern is broken up into small pieces. The phase angles of the velocities are erratic with respect to position in the array, with a total variation in phase of 4 degrees.

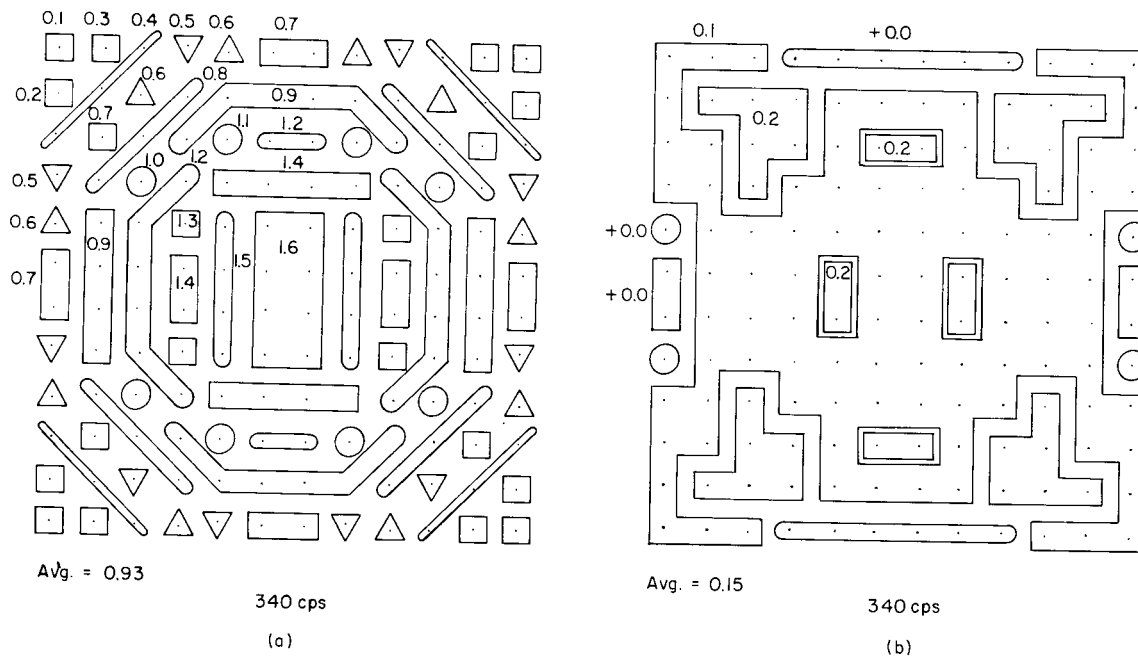


Fig. 20 - Contours of the (a) real and (b) imaginary parts of the radiation load for the 144-element array driven at 340 cps. The dots represent the positions of the transducer elements in the array. The data are for the connection 2 case (see Fig. 5).

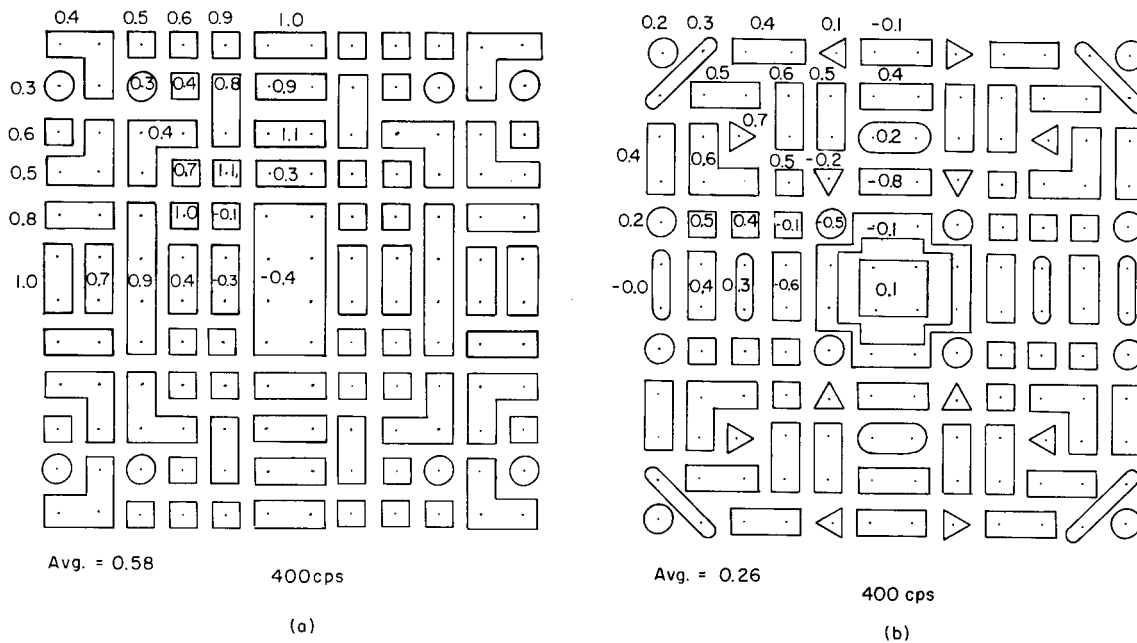


Fig. 21 - Contours of the (a) real and (b) imaginary parts of the radiation load for the 144-element array driven at 400 cps. The dots represent the positions of the transducer elements in the array. The data are for the connection 2 case (see Fig. 5).

Figure 22(a) presents the real part of the radiation load when the array is driven at a frequency of 450 cps. Note the large differences in the radiation load occurring between an edge element and an adjacent inner element. All elements except those located in an outer row and column have a large radiation load. The outer edge elements have the highest velocity magnitudes.

Figure 22(b) presents the imaginary part of the radiation load. The outer elements have the highest radiation load, decreasing to zero and becoming negative at the center of the array. The phase angles of the velocities are larger toward the center of the array, with a total variation of 57 degrees.

Figure 23 presents the real part of the radiation load, at a frequency of 400 cps, for the case where all of the velocities are equal, both in magnitude and phase. Note the progressive increase in the values of the radiation load from an edge toward the center of the array (lower right-hand corner). There is an order of magnitude variation in the values of the radiation load for the array.

Figure 24 presents the real part of the radiation load, at a frequency of 400 cps, for the case where there is a 180-degree reversal of the phase of the velocities between adjacent elements, with all the elements having equal velocity magnitudes. Note the alteration in sign of the real part of the radiation load, as well as the extremely small values of the load. This special problem is included in the report as an illustration of a way of obtaining an extremely poor radiation load, and hence very little radiated energy. The mathematical model for this case would approximate the situation where the physical array is a checkerboard arrangement of monopole and dipole radiators; that is, monopole radiators are on all the black squares and dipole radiators are on all the red squares. This would result in one surface (face) of the array having the normal impedance and the other surface (back) having a small real radiation load.

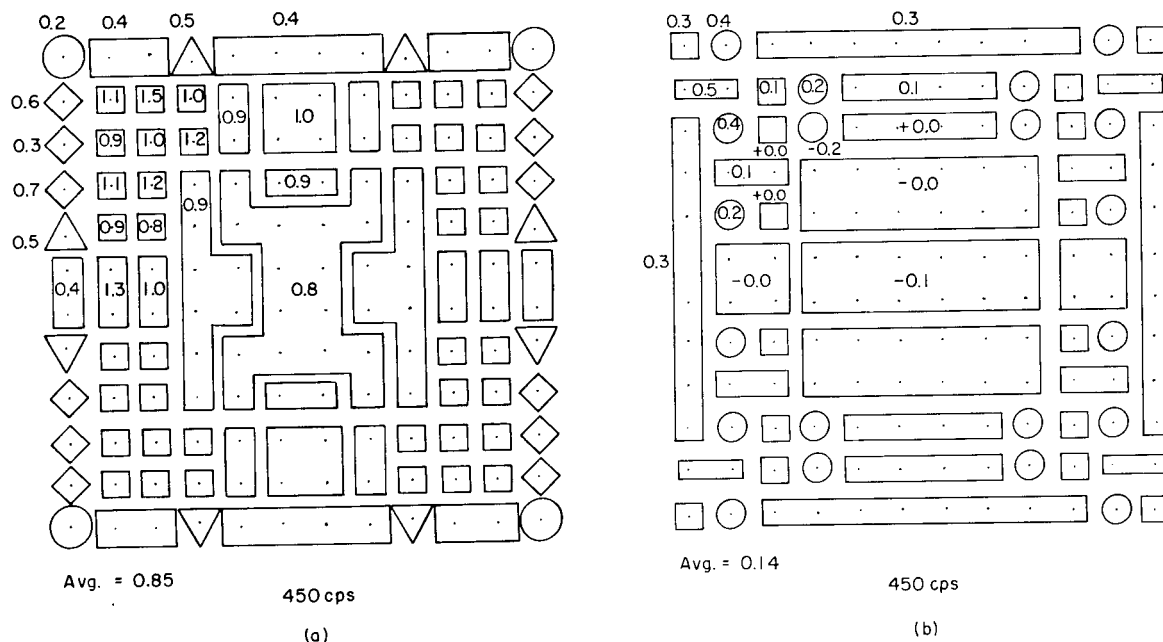


Fig. 22 - Contours of the (a) real and (b) imaginary parts of the radiation load for the 144-element array driven at 450 cps. The dots represent the positions of the transducer elements in the array. The data are for the connection 2 case (see Fig. 5).

.17	.28	.39	.48	.56	.59
.28	.43	.58	.72	.82	.87
.39	.58	.78	.95	1.07	1.14
.48	.72	.95	1.15	1.29	1.37
.56	.82	1.07	1.29	1.46	1.54
.59	.87	1.14	1.37	1.54	1.64

Avg. = 0.858

400 cps

Fig. 23 - Illustration of the values for the real part of the radiation load when each element in the array is driven with the same velocity, both in magnitude and phase. One-quarter of the array is shown, and each element is driven at 400 cps.

-.0036	.0042	-.0046	.0046	-.0046	.0045
.0042	-.0027	.00082	.0011	-.0026	.0034
-.0046	.00082	.0033	-.0071	.010	-.012
.0046	.0011	-.0071	.013	-.017	.019
-.0046	-.0026	.010	-.017	.022	-.025
.0045	.0034	-.012	.019	-.025	.028

Avg. = 0.0003

400 cps

Fig. 24 - Illustration of the values for the real part of the radiation load when adjacent elements in the array are driven 180 degrees out of phase, but with equal velocity amplitudes. One-quarter of the array is shown, and each element is driven at 400 cps.

SUMMARY

In summary, some general observations may be noted. The elements located near the outer edges of the 144-element transducer array have larger external mass velocity magnitudes, with a smooth, moderately well behaved frequency response. The phase of the velocity is moderately uniform over the frequency range investigated (340-500 cps). Many of the interior element peak responses have been shifted along the frequency axis with respect to the outer elements, and these shifts are in general toward a lower frequency. At the center of the square array, large variations occur in the magnitudes of the velocities with rapid changes in the phases of the velocities. The all-parallel connection (connection 1) curve, for many of the elements, has a pronounced dip near the air resonant frequency and a large peak above the air resonant frequency.

Comparisons of the internal mass velocity for the three types of electrical terminal connections (see Fig. 5) indicate that the elements near the edge of the array are more moderate in their behavior than the interior elements. The mass velocity curve for connection 1 is the least erratic, as a function of frequency, of the three curves. The closer the element is to the center of the array, the more erratic is the element behavior. In fact, for some of the elements near the center of the array, the velocity phase for the internal mass reverses its sign with respect to the phase of the external mass velocity, as it should when power is absorbed from the acoustic field.

The closer the element is to the center of the array, the more drastic are the peaks in the magnitude of the spring displacement. When the elements of the array are connected according to connection 3, the results are the least desirable. The phase of the spring displacement has very rapid changes as a function of frequency for the central

elements. The all-parallel connection has the most uniform spring displacements at the lower frequencies, and the connection 2 has the most uniform displacements at the higher frequencies.

With the exception of the central elements of the array, connection 2 radiates the largest peak power. Connection 1 has the most uniform power curve with, in general, the broadest bandwidth. All connections result in power being absorbed from the acoustic field at certain frequencies near the center of the array. Connections 2 and 3 absorb energy from the field at 400 cps, and connection 1 at 450 cps. Observations of the average power radiated do not provide any indications as to difficulties experienced by the individual elements. For the all-parallel arrangement the array has the lowest Q value and radiates the least amount of power per unit of averaged current.

When comparing the average real part of radiation load for the total array with respect to the different connections, the erratic behavior for connections 2 and 3 are similar and occur at a much lower frequency than for connection 1. The average imaginary part of the radiation load reveals a severe dip below 400 cps and, in addition, several other peaks and dips for connection 3.

The impedance plots for the individual elements indicate that the elements located on the perimeter are lightly loaded and that elements near the center of the array vary in load, from a condition of absorbing energy from the acoustic field, to a heavily loaded condition, depending on the frequency and the type of connection.

It was noted, when comparing the real part of the radiation load pattern for the three electrical terminal connections at the low-frequency end, that their "contours" are quite similar, with the all-parallel connection having the highest degree of circular symmetry. The magnitude of the velocities for all three are quite uniform at the low-frequency end. Even for a moderately uniform velocity distribution, there is an order of magnitude variation across the array in the real part of the radiation load.

It was noted, in comparing the imaginary components of the radiation load at the low-frequency end, that the all-parallel connection has the highest degree of circular symmetry, although connection 2 has the most uniform load. Phase comparisons of the velocities show the all-parallel to have the largest variation, with connection 2 having nearly a constant phase.

In making comparisons at 400 cps, the all-parallel radiation load contour still retains a circular symmetry even though the variations in values of the real part of the load have increased. Connection 3 case has some elements with large, negative, real radiation loads near the center of the array. Connection 2 case has many elements at the center of the array having negative real parts of radiation load. In addition, connection 2 contour of the real radiation load is completely devoid of any circular symmetry. The all-parallel connection (connection 1) has by far the largest average radiation load. The magnitude of the velocity and the phase angle are the most uniform for the all-parallel, whereas the magnitude of the velocity has the greatest variations for connection 2. Comparisons of the imaginary part of the radiation load at 400 cps show that all three connections demonstrate negative loads, with the larger negative loads appearing near the center of the array. The all-parallel has the least amount of variation, and connection 3 has the largest variation in the imaginary part of the load.

Comparisons at a frequency of 450 cps reveal that the all-parallel connection has the lowest average real part of radiation load, with a large negative load at the center of the array. Connection 2 plot has the largest average real part of radiation load, with a

moderately uniform load throughout the array, except for those elements that lie in the outer perimeter. Note that connection 2 has the largest variations in the magnitude of the velocities, with the all-parallel connection having the least amount of variations. Comparisons of the imaginary parts of the radiation load at a frequency of 450 cps show the connection 2 case to have the most uniform load, with the all-parallel having the highest average load. Phase comparisons show connection 2 and connection 3 to have similar variations, with the all-parallel (connection 1) having the greatest variations.

Computations have been made (and will be given in a later report) which show that a single series-connected capacitor for each array element whose value tunes the clamped reactance at 450 cps yields a reasonably well-behaved array over the entire band of frequencies when all elements are connected in parallel. That is, the negative real part of the radiation load is eliminated for all frequencies and the percentage variation in spring displacements is much improved. Therefore, a cure for the Artemis array is the connection of all elements in electrical parallel with a single-valued series capacitor for each element which is tuned at 450 cps.

ACKNOWLEDGMENTS

The required computer programs have been developed over a period of several years and are now rather extensive and flexible. We wish to express a sincere sense of gratitude to the NAREC Computation Group and, in particular, to Mrs. Janet Mason and Mr. Maurice Brinkman. This program permits modifying the physical problem in numerous interesting ways to obtain results for many parameters other than those presented here.

The bibliographic items listed below are included as a service to those who are interested in pursuing this field.

BIBLIOGRAPHY

1. Baier, R.V., "Evaluation of Effects of Element Interactions In a Large Low-Frequency Array," NRL Report 5251 (Confidential Report, Unclassified Title), Feb. 1959
2. Baier, R.V., "Evaluation of Effects of Interactions Among Non-Identical Elements In a Large Acoustic Array," NRL Report 5355 (Confidential Report, Unclassified Title), Sept. 1959
3. Baier, R.V., "Evaluation of Effects of Interactions For a Symmetrical Arrangement of Non-Identical Elements In a Large Acoustic Array," NRL Report 5491 (Confidential Report, Unclassified Title), July 1960
4. Barrett, E.L., "Mutual Radiation Impedance Coefficients For Identical Circular Pistons In a Stiff Infinite Plane Baffle," U.S. Navy Underwater Sound Laboratory, Tech. Memo. No. 1150-39-58, July 23, 1958
5. Alperin, H.A., "Mutual Radiation Impedance of Pistons (of $ka = 0.40$) Symmetrically Arranged In a Stiff Plane Baffle," U.S. Navy Underwater Sound Laboratory, Tech. Memo. No. 1150-64-56, June 13, 1956
6. Sherman, C.H., "Mutual Radiation Impedance Between Pistons On Spheres and Cylinders," U.S. Navy Underwater Sound Laboratory, Research Report No. 405, Nov. 24, 1958
7. Klapman, S.J., "Interaction Impedance of a System of Circular Pistons," J. Acoust. Soc. Am., 11:289-295 (1940)
8. Robey, D.H., "On the Radiation Impedance of an Array of Finite Cylinders," J. Acoust. Soc. Am., 27:706-710 (1955)
9. Swenson, G.W., Jr., and Johnson, W.E., "Radiation Impedance of a Rigid Square Piston in An Infinite Baffle," J. Acoust. Soc. Am., 24:84 (1952)
10. Hudimac, A.A., "Impedance of a Rigid Piston in An Infinite Rectangular Array of Pistons," Lorad Summary Report VI-59 (Confidential Report, Unclassified Title), Aug. 1953
11. Hanish, S., "A Survey of the Problem of Determining the Mutual-Interaction-Radiation Impedance of Individual Transducers In a Multitransducer Array" (Confidential Report, Unclassified Title), U.S. Navy J. Acoust., 10(No. 1):132-139 (1960)
12. Skorheim, R.D., "The Radiation Impedance of a Colinear Array of Finite Cylindrical Radiators," M.S. thesis, U.S. Naval Postgraduate School, 1957
13. Laird, D.T., and Cohen, H., "Directionality Patterns For Acoustic Radiation From a Source On a Rigid Cylinder," J. Acoust. Soc. Am., 24:46-49 (1952)
14. Martin, C.E., and Hickman, J.S., "Radiation Impedance of Large Low-Frequency Arrays Including the Lorad Mod. I Projector Array," U.S. Navy Electronics Laboratory, Report 698 (Confidential Report, Unclassified Title), pp. 68-77, June 1956

15. Hanish, S., "The Mechanical Self-Resistance and the Mechanical Mutual Resistance of An Unbaffled Rigid Disk ($ka < 1$) Radiating Sound From a Single Face Into an Acoustic Medium," NRL Report 5538, Oct. 1960
16. Hanish, S., "The Radiation Mechanical Impedance of Multizone Radiators In a Prolate Spheroidal Baffle," NRL Report 5515, Oct. 1960
17. Hanish, S., "The Mutual Mechanical Radiation Resistance For All Values of ka Of An Unbaffled Circular Rigid Piston With Pressure Released Back," NRL Report 5513, Sept. 1960
18. Karnovskii, M.I., "Calculation of the Radiation of Several Types of Distributed Radiator Systems," Soviet Phys. Acous. 2(No. 3):280-293 (1956)
19. "The Calculation of Mutual Acoustic Impedances," Collected works of the Kiev Cinema-Engineering Institute, 1:95-113 (1948)
20. Karnovsky, M.F., "Interaction Acoustical Impedance of Spherical Radiators and Resonators," Comptes Rendus (Doklady) de l'Academie des Sciences de l'URSS, 32 (No. 1):40-43 (1941)
21. Sherman, C.H., and Kass, D.F., "Radiation Impedances, Radiation Patterns, and Efficiency for a Large Array on a Sphere," U.S. Navy Underwater Sound Laboratory Research Report No. 429, July 1959
22. Lyon, R.H., "On the Low-Frequency Radiation Load of a Bass-Reflex Speaker" (letter to editor), J. Acoust. Soc. Am., 29:654 (1957)
23. Toulis, W.J., "Radiation Load on Arrays of Small Pistons," J. Acoust. Soc. Am., 29: 346-348 (1957)
24. Pritchard, R.L., "Mutual Acoustic Impedance Between Radiators In An Infinite Rigid Plane," J. Acoust. Soc. Am., 32:730-737 (1960)
25. Brillouin, J., "Rayonnement Transitoire Des Sources Sonores Et Problemes Connexes," Ann. Telecommun. (Cahiers d'Acoustique) 5(No. 13):160-172; 179-194 (1950)
26. Sherman, C.H., and Kass, D.F., "Near-Field Sound Pressure of Arrays of Pistons," U.S. Navy Underwater Sound Laboratory, Report No. 495, Feb. 1961
27. Urick, R.J., "Status Report for Radiation Impedance Study," Chesapeake Instrument Corp., Report No. 122, Sept. 1960
28. Simmons, B.D., "Radiation Impedance of Arrays of Finite Spherical Sources," Chesapeake Instrument Corp., Report No. 123, Aug. 1960
29. Sherman, C.H., "Example of Interaction Effects in Transducer Arrays. Part III," U.S. Navy Underwater Sound Laboratory, Tech. Memo. No. 912-82-62, Sept. 1962
30. Atwood, J.F., "Example of Interaction Effects in Transducer Arrays. Part II," U.S. Navy Underwater Sound Laboratory, Tech. Memo. No. 912-44-62, May 1962
31. Atwood, J.F., and Sherman, C.H., "Example of Interaction Effects In Transducer Arrays," U.S. Navy Underwater Sound Laboratory, Tech. Memo. No. 912-20-62, Mar. 1962

32. Allen, J.L., Cartledge, L., Delaney, W.P., DiBartalo, J., Siegel, M., Sinclair, G.R., Spaerri, S., Teele, J.H., and Temme, D.H., "Phased Array Radar Studies," Massachusetts Institute of Technology, Lincoln Laboratory Report No. 228, Aug. 1960
33. Mangulis, V., "Pistons On Corners," TRG, Inc., TRG-142-TN-63-3, Aug. 1963
- 34a. Rusby, J.S.M., "An Investigation of the Total Radiation Impedance of Rigid Piston Sound Sources in Arrays. Part I - The Experimental Technique," Great Britain, Admiralty Research Laboratory ARL/R27/L (Confidential Report, Unclassified Title), Aug. 1961
 - b. "Part II - Total Radiation Impedance Measurements Between Pairs of Rigid Pistons As a Function of Separation Distance," ARL/R28/L (Confidential Report, Unclassified Title), Aug. 1961
 - c. "Part III - Radiation Impedance Measurements On a Rigid Piston In a Baffle," ARL/R29/L (Confidential Report, Unclassified Title), Aug. 1961
 - d. "Part IV - Total Radiation Impedance Measurements On Rigid Pistons In Arrays," ARL/R30/L (Confidential Report, Unclassified Title), Aug. 1961
35. Kitz, B., and Crane, P.H.G., "An Assessment of the Relative Importance of Mutual Impedance In a Number of Transducer Array Designs," Great Britain, Admiralty Research Laboratory, ARL/L/N82 (Confidential), Dec. 1962
36. Merriweather, A.S., "An Experimental and Theoretical Verification of the Mutual Impedance Effect In Low-Frequency Underwater Acoustic Projector Arrays," Great Britain, Admiralty Research Laboratory, ARL/L/N78 (Confidential Report, Unclassified Title), Jan. 1963

CONFIDENTIAL

APPENDIX A

RELATIONS OF A SQUARE PISTON TO A CIRCULAR PISTON

If the square piston is replaced by a circular piston with a radius derived on the basis of an equal volume velocity of the square piston, then for closely spaced pistons the mathematical models would overlap. To avoid this possibility we replaced the square piston with a circular piston whose radius is the radius of a circle inscribed within the square piston. This inscribed radius is used to determine Pritchard's mutual impedance coefficients. These coefficients are then adjusted to compensate for the reduction in the area in the following manner. We compute the self-radiation impedance for the radius of the equal-volume-velocity circular piston and the radius of the inscribed circular piston. The ratio of the real part of the impedances, as determined by the equal-volume-velocity radius, to that of the inscribed radius is a multiplying factor for the real part of Pritchard's coefficients. Similarly, one obtains the ratio of the reactive impedances and multiplies the reactive part of Pritchard's coefficients. In addition, for the self-impedance we used the radius of the circle as determined by the equal volume velocity.

CONFIDENTIAL

CONFIDENTIAL

LIST OF SYMBOLS

- E = Voltage across the terminals of the amplifier.
- I_{Lk} = Current through any series grouping of elements (current entering element terminals).
- Z_{Lk} = Complex passive impedance quantity.
- Y_{Pk} = Complex passive admittance quantity.
- I_{Pk} = Current through Y_{Pk} admittance.
- E_{Lk} = Voltage across Y_{Pk} terminals.
- Z_{Ck} = "Clamped impedance" in air ($Z_{Ck} = 4 + j72$ ohms at 420 cps).
- E_{Tk} = Voltage across primary side of ideal transformer.
- I_{Tk} = Current through "clamped impedance."
- T = Turns ratio of ideal transformer ($T = 1.88 \times 10^9$ dynes/abamp).
- f_k = Force flowing through secondary of ideal transformer.
- y_{sk} = Mechanical unresponsiveness and unexcitability for the mechanical spring element.*
- y_{mr} = Immobility associated with the radiating mass* ($Y_{mr} = j\omega 42403.6$ gm/sec).
- y_{mi} = Immobility associated with the nonradiating mass ($Y_{mi} = j\omega 30236.4$ gm/sec).
- y_{rk} = Radiation load ($y_{rk} = G_r + jB_r$).
- u_{sk} = Velocity across the spring.
- u_{rk} = Velocity of radiating mass with respect to an inertial reference frame.
- $2x$ = Length of one side of the square array ($2x = 380$ cm).
- ρ = Density of the medium (gm/cm³).
- c = Velocity of sound in the medium (cm/sec).
- A = Area of the element face (cm²).
- \bar{a}^\dagger = Radius of the equal-volume-velocity circular piston ($\bar{a} = 16.88$ cm).

*See F. A. Firestone, "Twixt Earth and Sky with Rod and Tube," J. Acoust. Soc. Am. 28: 1126 (1956).

† See Appendix A.

a^{\dagger} = Radius of circle inscribed within the square piston ($a = 14.9606$ cm).

k = Wavenumber $2\pi/\lambda$

λ = Wavelength of sound in the medium (cm).

d_0 = Unit spacing of elements, center to center ($d_0 = 31.83$ cm).

The individual mechanical Q varies from 49 to 57 as a function of position in the array.
The resonant frequency in air of the individual elements varies from 443 to 454 cps.

~~CONFIDENTIAL~~

Security Classification

DOCUMENT CONTROL DATA - R&D

(Security classification of title, body of abstract and indexing annotation must be entered when the overall report is classified)

1. ORIGINATING ACTIVITY (Corporate author) U. S. Naval Research Laboratory Washington, D. C. 20390		2a. REPORT SECURITY CLASSIFICATION CONFIDENTIAL	
		2b. GROUP 4	
3. REPORT TITLE (Unclassified) THEORETICAL INTERACTION COMPUTATIONS FOR TRANSDUCER ARRAYS, INCLUDING THE EFFECTS OF SEVERAL DIFFERENT TYPES OF ELECTRICAL TERMINAL CONNECTIONS			
4. DESCRIPTIVE NOTES (Type of report and inclusive dates) Interim report			
5. AUTHOR(S) (Last name, first name, initial) Baier, R.V.			
6. REPORT DATE October 7, 1965		7a. TOTAL NO. OF PAGES 44	7b. NO. OF REFS 36
8a. CONTRACT OR GRANT NO. NRL Problem S02-07		9a. ORIGINATOR'S REPORT NUMBER(S) NRL Report 6314	
b. PROJECT NO. RF 101-03-44-4052		9b. OTHER REPORT NO(S) (Any other numbers that may be assigned this report) None	
c.			
d.			
10. AVAILABILITY/LIMITATION NOTICES			
11. SUPPLEMENTARY NOTES None		12. SPONSORING MILITARY ACTIVITY Dept. of the Navy (Office of Naval Research)	
13. ABSTRACT (Confidential) Mutual interactions between the elements of a transducer array affect the velocities, radiation loading, directivity patterns, and the internal electrical and mechanical stresses within the individual elements of a given array and element design. The effects are particularly serious and destructive where the individual elements are "close packed" and small in size compared to a wavelength. These interaction effects have been evaluated theoretically so as to include the electro-mechanical properties of each element, the array geometry, and several types of arrangements of the electrical terminals for a λ by λ (square) array composed of 144 individual radiators whose center frequency is 400 cps. The results of the computations are presented in terms of the theoretical velocities, radiation loading "contours," power radiated, electrical input impedance, and spring displacements. These results are compared for three different types of electrical terminal connections as a function of the driving frequency. Some of the more interesting results of the computations are the following. The elements located on the perimeter of the array have a much more uniform behavior with respect to frequency than the interior elements. The all-parallel connection, composed of one group of 144 elements all connected in parallel and denoted by (1,144), has the best performance at the lower frequencies, whereas the series-parallel (6,24) and the series-parallel (36,4) connections have the best performance at the high frequencies. All three types of electrical terminal connections are characterized by power absorption from the acoustic field at some frequency, but this effect occurs at different frequencies for the different types of electrical connections. The phases and the magnitudes of the velocities for these elements have rapid changes near the frequency where elements absorb power from the acoustic field. In all cases the series-parallel connection (6,24) is the worst offender.			

REF ID: A66700

CONFIDENTIAL
Security Classification

14.	KEY WORDS (Unclassified)	LINK A		LINK B		LINK C	
		ROLE	WT	ROLE	WT	ROLE	WT
	Transducers Interference Electrical networks Mathematical analysis (Interactions) Mutual coupling						

INSTRUCTIONS

1. **ORIGINATING ACTIVITY:** Enter the name and address of the contractor, subcontractor, grantee, Department of Defense activity or other organization (*corporate author*) issuing the report.
- 2a. **REPORT SECURITY CLASSIFICATION:** Enter the overall security classification of the report. Indicate whether "Restricted Data" is included. Marking is to be in accordance with appropriate security regulations.
- 2b. **GROUP:** Automatic downgrading is specified in DoD Directive 5200.10 and Armed Forces Industrial Manual. Enter the group number. Also, when applicable, show that optional markings have been used for Group 3 and Group 4 as authorized.
3. **REPORT TITLE:** Enter the complete report title in all capital letters. Titles in all cases should be unclassified. If a meaningful title cannot be selected without classification, show title classification in all capitals in parenthesis immediately following the title.
4. **DESCRIPTIVE NOTES:** If appropriate, enter the type of report, e.g., interim, progress, summary, annual, or final. Give the inclusive dates when a specific reporting period is covered.
5. **AUTHOR(S):** Enter the name(s) of author(s) as shown on or in the report. Enter last name, first name, middle initial. If military, show rank and branch of service. The name of the principal author is an absolute minimum requirement.
6. **REPORT DATE:** Enter the date of the report as day, month, year, or month, year. If more than one date appears on the report, use date of publication.
- 7a. **TOTAL NUMBER OF PAGES:** The total page count should follow normal pagination procedures, i.e., enter the number of pages containing information.
- 7b. **NUMBER OF REFERENCES:** Enter the total number of references cited in the report.
- 8a. **CONTRACT OR GRANT NUMBER:** If appropriate, enter the applicable number of the contract or grant under which the report was written.
- 8b, 8c, & 8d. **PROJECT NUMBER:** Enter the appropriate military department identification, such as project number, subproject number, system numbers, task number, etc.
- 9a. **ORIGINATOR'S REPORT NUMBER(S):** Enter the official report number by which the document will be identified and controlled by the originating activity. This number must be unique to this report.
- 9b. **OTHER REPORT NUMBER(S):** If the report has been assigned any other report numbers (*either by the originator or by the sponsor*), also enter this number(s).
10. **AVAILABILITY/LIMITATION NOTICES:** Enter any limitations on further dissemination of the report, other than those

imposed by security classification, using standard statements such as:

- (1) "Qualified requesters may obtain copies of this report from DDC."
- (2) "Foreign announcement and dissemination of this report by DDC is not authorized."
- (3) "U. S. Government agencies may obtain copies of this report directly from DDC. Other qualified DDC users shall request through _____."
- (4) "U. S. military agencies may obtain copies of this report directly from DDC. Other qualified users shall request through _____."
- (5) "All distribution of this report is controlled. Qualified DDC users shall request through _____."

If the report has been furnished to the Office of Technical Services, Department of Commerce, for sale to the public, indicate this fact and enter the price, if known.

11. **SUPPLEMENTARY NOTES:** Use for additional explanatory notes.
12. **SPONSORING MILITARY ACTIVITY:** Enter the name of the departmental project office or laboratory sponsoring (*paying for*) the research and development. Include address.
13. **ABSTRACT:** Enter an abstract giving a brief and factual summary of the document indicative of the report, even though it may also appear elsewhere in the body of the technical report. If additional space is required, a continuation sheet shall be attached.

It is highly desirable that the abstract of classified reports be unclassified. Each paragraph of the abstract shall end with an indication of the military security classification of the information in the paragraph, represented as (*TS*), (*S*), (*C*), or (*U*).

There is no limitation on the length of the abstract. However, the suggested length is from 150 to 225 words.
14. **KEY WORDS:** Key words are technically meaningful terms or short phrases that characterize a report and may be used as index entries for cataloging the report. Key words must be selected so that no security classification is required. Identifiers, such as equipment model designation, trade name, military project code name, geographic location, may be used as key words but will be followed by an indication of technical context. The assignment of links, roles, and weights is optional.